A FINITE DIFFERENCE SOLUTION FOR THE CYLINDRICAL EXPANSION OF A GAS CLOUD INTO VACUUM

by

F. Sherfield, J.H.S. Lee, and G.G. Bach

prepared for

NATIONAL AERONAUTICS AND SPACE ADMINISTRATION

CONTRACT NAS 3-4190

SPACE RESEARCH INSTITUTE
McGILL UNIVERSITY

NASA CR-54254

TOPICAL REPORT

A FINITE DIFFERENCE SOLUTION FOR THE CYLINDRICAL EXPANSION OF A GAS CLOUD INTO VACUUM

by

I. Shanfield, J.H.S. Lee, and G.G. Bach

prepared for

NATIONAL AERONAUTICS AND SPACE ADMINISTRATION

March 15, 1965

CONTRACT NAS 3-4190

Technical Management
NASA Lewis Research Center
Cleveland, Ohio
Liquid Rocket Technology Branch
Gordon T. Smith

SPACE RESEARCH INSTITUTE
McGill University
892 Sherbrooke St. W.
Montreal 2, Canada

19702

SUMMARY

A finite difference method for the solution of an axi-symmetric expansion of a perfect gas into vacuum is developed. The method is applied to the expansion of a gas with an equation of state of the form of Tillotson's equation. The solution obtained by the finite difference method for a perfect gas expansion is compared to the characteristic solution to check the validity of the finite difference method. A similarity solution for the perfect gas expansion is compared to the long-term finite difference solution.

AUTHOR ↑

ACKNOWLEDGEMENTS

The authors wish to thank Prof. G.V. Bull for his initiation of the problem. Thanks are due to Mr. F.J. Zwarts who developed the program for the solution of the expansion by the characteristic method. The support of NASA, under contract number NAS3-4190, is acknowledged.

LIST OF SYMBOLS

Non-Dimensional Variables

a	speed of sound
a, b, α, β	constants in Tillotson's equation (Eqs. 6.3 and 6.4)
B	constant defined by Eq. 5.20
$c_1, c_2 \ldots c_7$	constants in polynomial $p = f(\rho)$
$d_1, d_2 \ldots d_7$	constants in polynomial $a = f(\rho)$
D	constant defined by Eq. 5.2
E	internal energy
$g_1, g_2, \ldots$	constants in polynomial $\rho = f\left(\frac{\tau-1}{\Delta}\right)$
p	pressure
r	radius
R	radius of escape front
s	entropy
t	time
u	particle velocity
u_f	escape front velocity
Δ	starting time
γ	specific heat ratio
ν	0 for plane expansion 1 for cylindrical expansion 2 for spherical expansion

λ_1	right-running characteristic
λ_2	left-running characteristic
ρ	density
σ	shock strength

Subscripts

av	linear average value of property between two points
c	state at which perfect gas relation becomes valid
es	property at the escape front
ex	property at the expansion front
f	escape front wave velocity
g	state at which condensation begins
o	undisturbed state
s	shocked state

Dimensioned Variables

$\overline{a}$	speed of sound, cm/sec
$\overline{A}$, $\overline{B}$	constants in Tillotson's equation of state (Eq. 6.3 and 6.4) dynes/cm^2
$\overline{E}$	internal energy, dyne cm/gm
$\overline{E}_o$	undisturbed internal energy, dyne cm/gm
$\overline{E}_s$	internal energy of shocked state, dyne cm/gm
$\overline{E}_g$	Internal energy at which condensation begins, dyne cm/gm
$\overline{p}$	Pressure dynes/cm^2

$\bar{r}$	radius, cm
$\bar{R}_o$	initial radius of expansion, cm
$\bar{s}$	entropy, dyne cm/gm^oK
$\bar{t}$	time, seconds
$\bar{T}$	temperature, ^oK
$\bar{u}$	particle velocity, cm/sec
$\bar{\rho}$	density, gms/cm^3
$\bar{\rho}_c$	density at which perfect gas relation becomes valid.

TABLE OF CONTENTS

TABLE OF CONTENTS cont'd

TABLE OF CONTENTS cont'd

1. INTRODUCTION

The complete description of the physics of the problem of the hypervelocity impact of a cylindrical pellet with a thin bumper plate has been described in an earlier report by Bull [1]. Due to the complexities of the various physical mechanisms involved and their interactions with one another, the method of approach toward a complete numerical solution of the impact model will be to investigate each mechanism separately and then to compile them together step by step to form the final complete model. To adequately describe the phenomena involved, a numerical technique in three independent variables, (two space variables and the time variable) must be developed. In this report, the first phase of the analytical program on the development of a finite difference method in one space variable for the solution of the radial expansion of a cylindrical gas cloud into a vacuum is presented. Provisions are made in the program such that any arbitrary equation of state can be used and numerical solutions for two cases of impact of aluminum pellets with aluminum bumpers using Tillotson's [2] equation of state are given. The finite difference solutions are checked against the characteristic solutions for a few cases to determine the accuracy of the solutions.

1.1. The Problem

The physical model consists of an infinitely long cylindrical gas cloud with a uniform density distribution at time

t = 0. At later times the gas cloud is allowed to expand into a vacuum. The problem involves only one spatial variable r; hence both the characteristic method and the finite difference method are straight forward. However, the finite difference approach is easier to handle when two spatial variables are involved. Existing solutions for this problem are of the similarity type which hold only under two particular conditions; (i) when the initial density distribution in the gas cloud is a particular function of r; [3] (ii) At very large times when the flow is inertia dominated for the case of an initially uniform density distribution [4]. Hence the solutions by the present method can be checked against the similarity solution of case (ii).

2. ANALYSIS

2.1. Equations of Motion

The basic equations governing the isentropic expansion of a gas can be written as:

Continuity: $$\frac{\partial \bar{\rho}}{\partial \bar{t}} + \bar{\rho} \frac{\partial \bar{u}}{\partial \bar{r}} + \bar{u} \frac{\partial \bar{\rho}}{\partial \bar{r}} + j \frac{\bar{\rho} \bar{u}}{\bar{r}} = 0 \qquad 2.1$$

Momentum: $$\frac{\partial \bar{u}}{\partial \bar{t}} + \bar{u} \frac{\partial \bar{u}}{\partial \bar{r}} + \frac{\bar{a}^2}{\bar{\rho}} \frac{\partial \bar{\rho}}{\partial \bar{r}} = 0 \qquad 2.2$$

The first law of thermodynamics for a particle is

$$\bar{T}\, d\bar{s} = d\bar{E} + \bar{p}\, d\left(\frac{1}{\bar{\rho}}\right) \qquad 2.3$$

where $j = 0$ for a plane expansion

$j = 1$ for a cylindrical expansion

$j = 2$ for a spherical expansion

The bar (-) above the physical quantities in Eq. 2.1 to 2.3 indicate that these quantities have dimensions.

Since an isentropic expansion is considered,

$$d\bar{s} = 0$$

and Eq. 2.3 is written as

$$d\bar{E} = \frac{\bar{p}}{\bar{\rho}^2}\, d\bar{\rho} \qquad 2.4$$

This equation may be integrated to yield

$$\bar{E} = \bar{E}_0 - \int_{\bar{\rho}}^{\bar{\rho}_s} \frac{\bar{p}}{\bar{\rho}^2}\, d\bar{\rho} \qquad 2.5$$

For a perfect gas, the equation of an isentrope is

$$\frac{\bar{p}}{\bar{\rho}^{\gamma}} = \text{const.} \qquad 2.6$$

and the speed of sound is given by

$$\bar{a}^2 = \gamma \frac{\bar{p}}{\bar{\rho}} \qquad 2.7$$

For a non-perfect gas, the equation of state is of the form

$$\bar{p} = \mathcal{J}(\bar{\rho}, \bar{E}) \qquad 2.8$$

and Eq. 2.5 must be integrated to obtain the pressure at each value of density.

2.2. Non-Dimensionalization of Basic Equations

In order to facilitate the numerical analysis, it is convenient to write the basic equations in non-dimensional form.

Setting:

$$\left.\begin{aligned} \rho &= \bar{\rho}/\bar{\rho}_s \\ u &= \bar{u}/\bar{a}_s \\ a &= \bar{a}/\bar{a}_s \\ r &= \bar{r}/\bar{R}_0 \\ t &= \bar{a}_s \bar{t}/\bar{R}_0 \end{aligned}\right\} \qquad 2.9$$

Eqs. 2.1 and 2.2 become:

$$\frac{\partial \rho}{\partial t} + \rho \frac{\partial u}{\partial x} + u \frac{\partial \rho}{\partial x} + j \frac{\rho u}{r} = 0 \qquad 2.10$$

$$\frac{\partial u}{\partial t} + u \frac{\partial u}{\partial x} + \frac{a^2}{\rho} \frac{\partial \rho}{\partial x} = 0 \qquad 2.11$$

3. CHARACTERISTIC SOLUTION FOR PERFECT GAS

3.1. Characteristic Relations:

A solution of the expansion by the method of characteristics is obtained for later comparison to the finite difference solution which is developed. The relations along a λ_1 and λ_2 characteristic line can be written as:

$$\lambda_1: \qquad \frac{dr}{dt} = u + a \tag{3.1}$$

$$du + \frac{1}{\rho a}\, dp = -j \frac{a u}{r}\, dt \tag{3.2}$$

$$\lambda_2: \qquad \frac{dr}{dt} = u - a \tag{3.3}$$

$$-du + \frac{1}{\rho a}\, dp = -j \frac{a u}{r}\, dt \tag{3.4}$$

and together with the isentropic and the speed of sound relationships,

$$\frac{\bar{p}}{\bar{\rho}^{\gamma}} = \text{const.} \tag{3.5}$$

$$\bar{a}^2 = \gamma \frac{\bar{p}}{\bar{\rho}} \tag{3.6}$$

Eqs. 2.10 and 2.11 can be integrated numerically along the characteristic paths.

3.2 Finite Difference Approximation

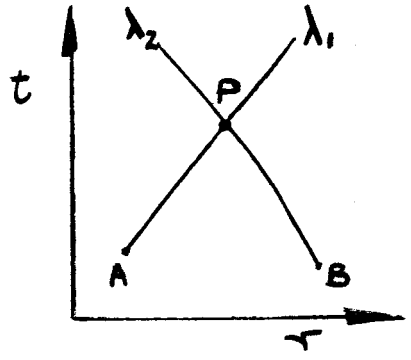

Fig. 3.1

Referring to Fig. 3.1, Eqs 3.1 to 3.4 can be written in finite difference form. If the grid points are sufficiently close together, the dependent variables can be assumed to vary linearly between the adjacent points. Eqs. 3.1 to 3.4 then become in the first order linear approximation:

$$\tau_P - \tau_A = (\mu+a)_{\lambda_1}(t_P - t_A) \qquad 3.7$$

$$u_P - u_A = -\left(\frac{1}{\rho a}\right)_{\lambda_1}(p_P - p_A) - j\left(\frac{au}{\tau}\right)_{\lambda_1}(t_P - t_A) \qquad 3.8$$

$$\tau_P - \tau_B = (\mu-a)_{\lambda_2}(t_P - t_B) \qquad 3.9$$

$$u_P - u_B = \left(\frac{1}{\rho a}\right)_{\lambda_2}(p_P - p_B) + j\left(\frac{au}{\tau}\right)_{\lambda_2}(t_P - t_B) \qquad 3.10$$

Eliminating τ_P from Eqs. 3.7 and 3.9

$$t_P = \frac{\tau_B - \tau_A + (\mu+a)_{\lambda_1} t_A - (\mu-a)_{\lambda_2} t_B}{(\mu+a)_{\lambda_1} + (\mu-a)_{\lambda_2}} \qquad 3.11$$

Re-arranging Eq. 3.7

$$\tau_P = \tau_A + (\mu+a)_{\lambda_1}\left(t_P - t_A\right) \qquad 3.12$$

Eliminating p_P from Eqs. 3.3 and 3.10

$$u_P = \frac{(\rho a)_{\lambda_1} u_A + (\rho a)_{\lambda_2} u_B + p_A - p_B + (\rho a)_{\lambda_2} j\left(\frac{\partial u}{\partial \tau}\right)_{\lambda_2}(t_P - t_B) - (\rho a)_{\lambda_1} j\left(\frac{\partial u}{\partial \tau}\right)_{\lambda_1}(t_P - t_A)}{(\rho a)_{\lambda_1} + (\rho a)_{\lambda_2}} \qquad 3.13$$

Re-arranging Eq. 3.8

$$p_P = p_A - (\rho a)_{\lambda_1}(u_P - u_A) - (\rho a)_{\lambda_1} j\left(\frac{\partial u}{\partial \tau}\right)_{\lambda_1}(t_P - t_A) \qquad 3.14$$

If the properties at points A and B are known, then t_P, τ_P, u_P and p_P can be found from Eqs. 3.11 to 3.14. The values of a_P and ρ_P can then be determined from Eqs. 3.5 and 3.6. A more detailed outline of the numerical procedure (including a second order approximation) is given in Section 7.1.

3.3. Boundary Conditions

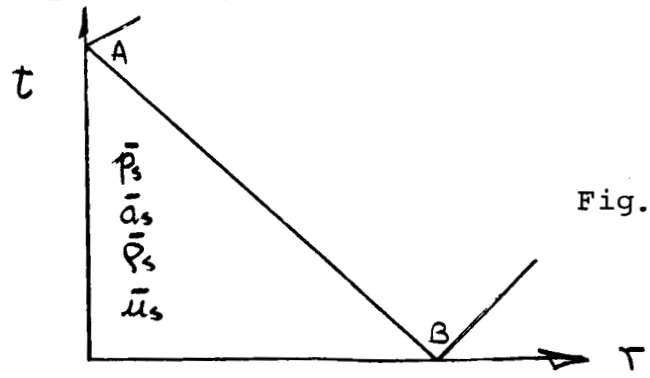

Fig. 3.2

The boundary conditions at the head of the expansion front AB (Fig. 3.2) which must be satisfied are as follows:

$$\left.\begin{aligned} u_{ex} &= \bar{u}_{ex}/\bar{a}_s = 0 \\ a_{ex} &= \bar{a}_{ex}/\bar{a}_s = 1 \\ \rho_{ex} &= \bar{\rho}_{ex}/\bar{\rho}_s = 1 \\ p_{ex} &= \bar{p}_{ex}/\bar{\rho}_s \bar{a}_s^2 = \bar{p}_s/\bar{\rho}_s \bar{a}_s^2 \end{aligned}\right\} \quad 3.15$$

where the subscript "ex" refers to values of the properties at the expansion front.

3.4 Treatment At The Center

In order to avoid the singularity in the term $j\frac{au}{r}$ (in Eqs. 3.2 and 3.4) as $r \to 0$, a slender rod of radius 0.0001 times the radius of the initial gas cloud is placed in the flow. The detailed numerical procedure for calculating points at the center is given in Section 7.1.

4. FINITE DIFFERENCE SOLUTION FOR PERFECT GAS

4.1 Basic Equations

For the solution of the expansion of a perfect gas by the finite difference method, the isentropic relation (Eq. 2.6) and Eq. 2.7 are used to transform Eqs. 2.10 and 2.11 to the following forms:

$$\frac{2}{\gamma-1}\frac{\partial a}{\partial t} + a\frac{\partial u}{\partial r} + \frac{2}{\gamma-1}u\frac{\partial a}{\partial r} + j\frac{au}{r} = 0 \qquad 4.1$$

$$\frac{\partial u}{\partial t} + u\frac{\partial u}{\partial r} + \frac{2}{\gamma-1}a\frac{\partial a}{\partial r} = 0 \qquad 4.2$$

Equations 4.1 and 4.2 can be re-arranged to yield the time derivatives of the variables "a" and "u" in terms of the spatial derivatives of the same variables and the values of these variables.

$$\frac{\partial a}{\partial t} = \frac{\gamma-1}{2}\left[-a\frac{\partial u}{\partial r} - \frac{2}{\gamma-1}u\frac{\partial a}{\partial r} - j\frac{au}{r}\right] \qquad 4.3$$

$$\frac{\partial u}{\partial t} = -u\frac{\partial u}{\partial r} - \frac{2}{\gamma-1}a\frac{\partial a}{\partial r} \qquad 4.4$$

4.2 Numerical Determination of The Derivatives

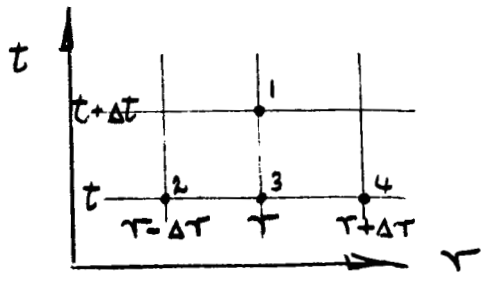

Fig. 4.1

In order to proceed with the finite difference solution, the derivatives of the fluid properties at the point (r,t) must be obtained. Assuming that the properties are known for all values of r at time t, one can write:

$$\frac{\partial}{\partial r} u(r,t) = \frac{u(r+\Delta r,t) - u(r-\Delta r,t)}{2\Delta r} \qquad 4.5$$

$$\frac{\partial}{\partial r} a(r,t) = \frac{a(r+\Delta r,t) - a(r-\Delta r,t)}{2\Delta r} \qquad 4.6$$

The values of $\frac{\partial}{\partial t} a(r,t)$ and $\frac{\partial}{\partial t} u(r,t)$ can now be found from Eqs. 4.3 and 4.4 using the values of a(r,t), u(r,t) and the values of $\frac{\partial}{\partial r} u(r,t)$ and $\frac{\partial}{\partial r} a(r,t)$ evaluated from Eqs. 4.5 and 4.6.

One can also write the following finite - difference relationships:

$$\frac{\partial u}{\partial t}(r,t) = \frac{1}{\Delta t}\left\{u(r,t+\Delta t) - \frac{1}{2}\left[u(r-\Delta r,t) + u(r+\Delta r,t)\right]\right\} \qquad 4.7$$

$$\frac{\partial a}{\partial t}(r,t) = \frac{1}{\Delta t}\left\{a(r,t+\Delta t) - \frac{1}{2}\left[a(r-\Delta r,t) + a(r+\Delta r,t)\right]\right\} \qquad 4.8$$

Eqs. 4.7 and 4.8 can be re-arranged as follows:

$$u(r,t+\Delta t) = \Delta t \frac{\partial}{\partial t} u(r,t) + \frac{1}{2}\left[u(r-\Delta r,t) + u(r+\Delta r,t)\right] \qquad 4.9$$

$$a(r,t+\Delta t) = \Delta t \frac{\partial}{\partial t} a(r,t) + \frac{1}{2}\left[a(r-\Delta r,t) + a(r+\Delta r,t)\right] \quad 4.10$$

Values for $\mu(r, t + \Delta t)$ and $a(r, t + \Delta t)$ are now determined:

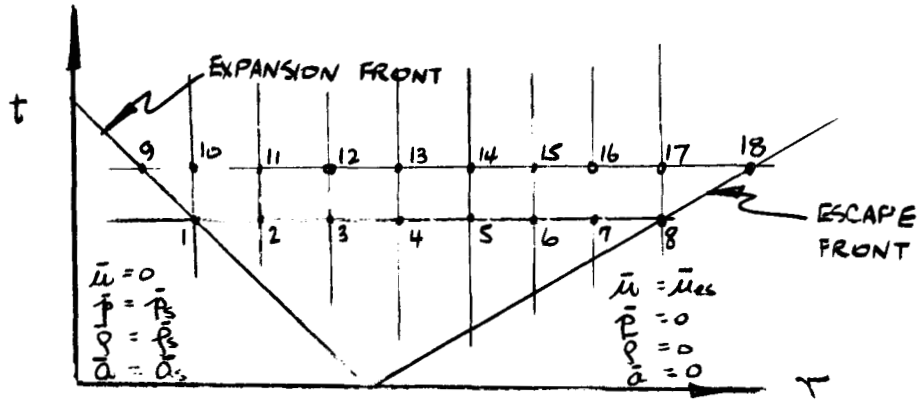

Fig. 4.2

By the above procedure, the properties at points 11 to 16 (Fig. 4.2) can be found from the known values of the properties at points 1 through 8. The properties at points 9 and 18 are known. Since the boundary conditions at the expansion front and at the escape front are known (Section 4.3) , the properties at point 10 can be found by linear interpolation between points 9 and 11, and those at point 17 by linear interpolation between points 16 and 18. Further interpolation must take place if the expansion or escape fronts do not pass through a grid point, but this will be clarified in Section 7.2.

4.3 Boundary Conditions

The boundary conditions at the expansion and escape fronts for a perfect gas can be expressed as:

$$\left.\begin{aligned} u_{ex} &= \bar{u}_{ex} / \bar{a}_s = 0 \\ a_{ex} &= \bar{a}_{ex} / \bar{a}_s = 1 \\ \rho_{ex} &= \bar{\rho}_{ex} / \bar{\rho}_s = 1 \\ p_{ex} &= \bar{p}_{ex} / \bar{\rho}_s \bar{a}_s^2 = \bar{p}_s / \bar{\rho}_s \bar{a}_s^2 \end{aligned}\right\} \qquad 4.11$$

$$\left.\begin{aligned} u_{es} &= \bar{u}_{es} / \bar{a}_s = \frac{2}{\gamma - 1} \\ a_{es} &= \bar{a}_{es} / \bar{a}_s = 0 \\ \rho_{es} &= \bar{\rho}_{es} / \bar{\rho}_s = 0 \\ p_{es} &= \bar{p}_{es} / \bar{\rho}_s \bar{a}_s^2 = 0 \end{aligned}\right\} \qquad 4.12$$

where the subscript "ex" refers to properties at the expansion front, and "es" to properties at the escape front.

4.4. Treatment At The Center

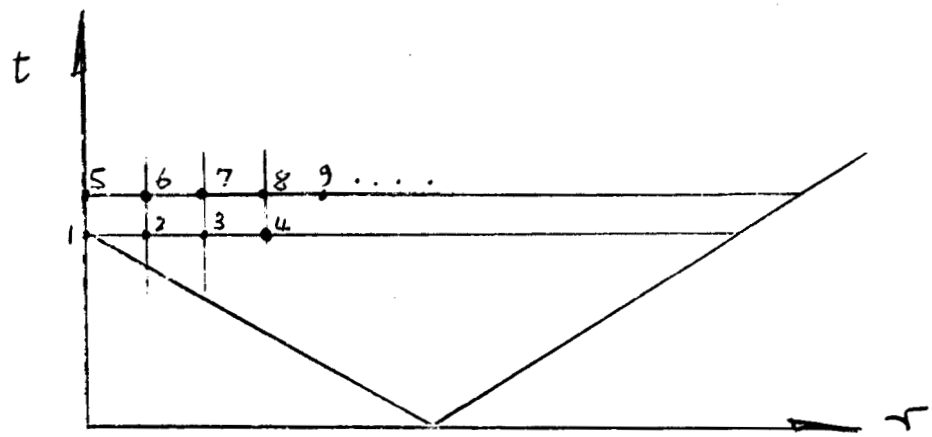

Fig.4.3

Once the properties at t = 1 have been determined (points 1, 2, 3.....in Fig. 4.3) it remains to find the properties at t = 1 + Δ t (points 5, 6, 7.....). At the center where r = 0, u is an odd function of r and a is an even function of r.

$$u(\Delta r) = -u(-\Delta r) \qquad 4.13$$

$$a(\Delta r) = a(-\Delta r) \qquad 4.14$$

The spatial derivatives of u and a are therefore

$$\left.\frac{\partial u}{\partial r}\right|_{r=0} = \frac{u(\Delta r) - u(-\Delta r)}{2\Delta r} = \frac{u(\Delta r)}{\Delta r} \qquad 4.15$$

$$\left.\frac{\partial a}{\partial r}\right|_{r=0} = \frac{a(\Delta r) - a(-\Delta r)}{2\Delta r} = 0 \qquad 4.16$$

The term $\frac{au}{r}$ in Eq. 4.1 has a limit at r = 0.

$$\lim_{r \to 0} \frac{au}{r} = \lim_{r \to 0} \frac{\frac{\partial}{\partial r}(au)}{\frac{\partial}{\partial r}(r)} = a \frac{\partial u}{\partial r} = \frac{a u(\Delta r)}{\Delta r} \quad 4.17$$

$\left.\frac{\partial a}{\partial t}\right|_1$ can be found from Eq. 4.3 using Eqs. 4.15, 4.16 and 4.17 and the known properties at 1.

$\left.\frac{\partial u}{\partial t}\right|_1$ can similarly be found from Eq. 4.4.

Eqs. 4.9 and 4.10 can be re-written for the case r = 0 using Eqs. 4.13 and 4.14.

$$u(0, t+\Delta t) = \Delta t \frac{\partial u}{\partial t}(0, t) \quad 4.13$$

$$a(0, t+\Delta t) = \Delta t \frac{\partial a}{\partial t}(0, t) + a(\Delta r, t) \quad 4.19$$

For point 5 therefore,

$$u(5) = \Delta t \left.\frac{\partial u}{\partial t}\right|_1 \quad 4.20$$

$$a(5) = \Delta t \left.\frac{\partial a}{\partial t}\right|_1 + a(2) \quad 4.21$$

where $\left.\frac{\partial u}{\partial t}\right|_1$ is found from Eqs. 4.4, 4.15 and 4.16.

$$\left.\frac{\partial u}{\partial t}\right|_1 = -u(1) \frac{u(2)}{\Delta r} - \frac{2}{\gamma - 1} a(1) \left.\frac{\partial a}{\partial r}\right|_1$$

Since $u(1) = 0$ and $\left.\frac{\partial a}{\partial r}\right|_1 = 0$,

$$\left.\frac{\partial u}{\partial t}\right|_1 = 0 \qquad 4.22$$

$\left.\frac{\partial a}{\partial t}\right|_1$ is found from Eqs. 4.3, 4.15, 4.16 and 4.17

$$\left.\frac{\partial a}{\partial t}\right|_1 = \frac{\gamma-1}{2}\left[-a(1)\frac{u(2)}{\Delta r} - \frac{2}{\gamma-1}u(1)\left.\frac{\partial a}{\partial r}\right|_1 - j\frac{a(1)u(2)}{\Delta r}\right]$$

$$\left.\frac{\partial a}{\partial t}\right|_1 = -\frac{\gamma-1}{2}(1+j)\frac{a(1)u(2)}{\Delta r} \qquad 4.23$$

The properties at points 6, 7, 8.... are found as outlined in Section 4.2. The properties at the center for successive times can be found in identically the same manner.

4.5 Starting Conditions For Perfect Gas

Due to the uniform density distribution at time t = 0, the density gradient is infinite at radius r = 1, and a numerical determination of the properties at a subsequent time cannot be obtained. In order to carry out the numerical solution of the gaseous expansion, the starting conditions at a time t = Δ must be evaluated. The flow is assumed to be one-dimensional for this small time increment, and the λ_1 and λ_2 characteristic equations (Eq. 3.1 to 3.4) are utilized.

$$\lambda_1: \quad \frac{d\tau}{dt} = u + a \; ; \quad du + a\frac{d\rho}{\rho} = 0 \qquad 4.24$$

$$\lambda_2: \quad \frac{d\tau}{dt} = u - a \; ; \quad -du + a\frac{d\rho}{\rho} = 0 \qquad 4.25$$

For a perfect gas

$$\lambda_1: \quad \frac{d\tau}{dt} = u + a \; ; \quad du + \frac{2}{\gamma - 1} da = 0 \qquad 4.26$$

$$\lambda_2: \quad \frac{d\tau}{dt} = u - a \; ; \quad -du + \frac{2}{\gamma - 1} da = 0 \qquad 4.27$$

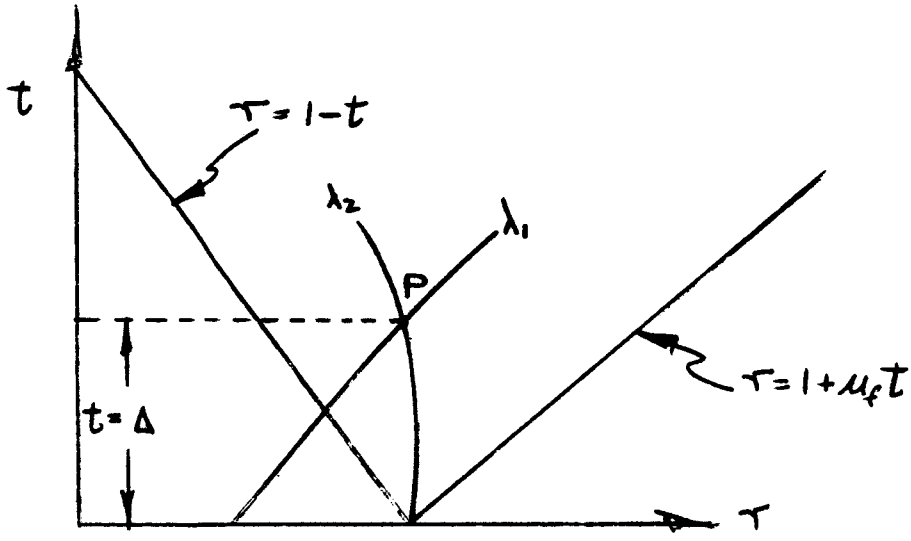

Fig. 4.4

Integrating along the λ_1 characteristic which passes through the point P (Fig. 4.4)

$$\int_0^u du = -\frac{2}{\gamma-1}\int_1^a da$$

$$u = \frac{2}{\gamma-1}(1-a) \qquad 4.28$$

Along the λ_2 characteristic through P

$$\int_1^\tau d\tau = \int_0^\Delta (u-a)\,dt$$

$$\tau - 1 = (u-a)\,\Delta \qquad 4.29$$

Combining Eqs. 4.28 and 4.29

$$a = \frac{2}{\gamma+1} - \frac{\gamma-1}{\gamma+1}\left(\frac{\tau-1}{\Delta}\right) \qquad 4.30$$

$$u = \frac{2}{\gamma+1}\left[1 + \frac{\tau-1}{\Delta}\right] \qquad 4.31$$

The distributions of u and a as functions of r can be obtained at the starting time Δ using Eqs. 4.30 and 4.31. The finite difference solution can then be continued as in Section 4.2.

It can be seen that the boundary conditions at both the escape front and the expansion front are satisfied. At the escape front

$$\tau = 1 + u_f \Delta$$

$$a_{es} = \frac{2}{\gamma+1} - \frac{\gamma-1}{\gamma+1} u_f$$

Since $u_f = \frac{2}{\gamma-1}$, $a_{es} = 0$

$$u_{es} = \frac{2}{\gamma+1}\left[1 + u_f\right] = \frac{2}{\gamma-1}$$

The boundary conditions at the escape front are therefore both satisfied.

At the expansion front, $r = 1 - \Delta$

$$a_{ex} = \frac{2}{\gamma+1} - \frac{\gamma-1}{\gamma+1}(-1) = 1$$

$$u_{ex} = \frac{2}{\gamma+1}\left[1-1\right] = 0$$

The boundary conditions are therefore satisfied at the expansion front as well.

5. SIMILARITY SOLUTION FOR PERFECT GAS WITH UNIFORM INITIAL DENSITY DISTRIBUTION

5.1. Basic Relations

It is desired to obtain a similarity solution for the long-term expansion of a gas with an initially uniform density distribution. Following the analysis of Ref. 4, the equations of mass and momentum conservation (Eqs. 2.1 and 2.2) can be written using the isentropic relation (Eq. 2.6) as

$$\frac{\partial \rho}{\partial t} + \frac{\partial}{\partial r}(\rho u) + j\frac{\rho u}{r} = 0 \qquad 5.1$$

$$\frac{\partial u}{\partial t} + u\frac{\partial u}{\partial r} + \rho^{\gamma-2}\frac{\partial \rho}{\partial r} = 0 \qquad 5.2$$

The pressure gradient term in the momentum equation (the last term of Eq. 5.2) becomes negligable after long time and Eq. 5.2 can then be integrated to yield

$$u = \frac{r}{t} \qquad 5.3$$

Substitution of Eq. 5.3 into Eq. 5.1 shows that the density distribution must have the form

$$\rho t^{j+1} = f\left(\frac{r}{t}\right) \qquad 5.4$$

The precise form of this function depends on the earlier motion of the gas cloud. The motion is self-similar (after long times) since both u and $\rho t^{\gamma+1}$ are functions only of $\frac{r}{t}$.

5.2 Self-Similar Flows

Looking at an expansion flow which is self-similar at all times, let us assume that R(t) is the leading edge of the gas cloud which is expanding into vacuum. The gas is contained in the region $0 \leq r \leq R(t)$. A simlarity variable is defined as

$$\eta = \frac{r}{R(t)} \qquad 5.5$$

so that the leading edge of the gas cloud corresponds to $\eta = 1$. Self-similar solutions are found by assuming the forms of the dependent variables.

$$u = g(t)\,\phi(\eta) \qquad 5.6$$

$$\rho = \ell(t)\,f(\eta) \qquad 5.7$$

Substituting Eqs. 5.6 and 5.7 into Eqs. 5.1 and 5.2 (neglecting the pressure gradient term of Eq. 5.2) and

finding the forms of g(t) and h(t) such that the resulting equations are independent of t, one obtains

$$\rho = R^{-(j+1)} \left[1 - \eta^2\right]^{\frac{1}{1-\gamma}} \qquad 5.8$$

$$u = \left(\frac{dR}{dt}\right) \eta \qquad 5.9$$

where $$\frac{dR}{dt} = \frac{1}{(j+1)^{1/2}} \frac{2}{\gamma - 1} \left[1 - R^{-(j+1)(\gamma-1)}\right]^{\frac{1}{2}} \qquad 5.10$$

This solution satisfies the following boundary conditions:

$$\left.\begin{array}{lll} t = 0 & R = 1 & \frac{dR}{dt} = 0 \\ t = 0 & r = 0 & \rho = 1 \\ t > 0 & \eta = 1 & \rho = 0 \\ t > 0 & \eta = 0 & u = 0 \end{array}\right\} \qquad 5.11$$

Thus initially (r = 0), u = 0 and ρ varies from 1 at r = 0 to 0 at R = r.

The location of the leading edge of the expansion can be found by integrating Eq. 5.10

$$\frac{1}{(j+1)^{1/2}} \frac{2}{\gamma - 1} t = \int_0^R \frac{dR}{\left[1 - R^{-(j+1)(\gamma-1)}\right]^{1/2}} \qquad 5.12$$

After long time , $R^{-(j+1)(\gamma-1)} \ll 1$, so that Eq. 5.12 may be written

$$\frac{1}{(j+1)^{1/2}} \frac{2}{\gamma-1} t = \int_0^R dR = R$$

ie $$R = \frac{1}{(j+1)^{1/2}} \frac{2}{\gamma-1} t \qquad 5.13$$

The velocity and density distributions can now be found from Eq. 5.3 and 5.9 as

$$\rho t^{j+1} = \left[\frac{(j+1)^{\frac{1}{2}}(\gamma-1)}{2}\right]^{j+1} \left(1-\eta^2\right)^{\frac{1}{\gamma-1}} \qquad 5.14$$

$$u = \frac{r}{t} \qquad 5.15$$

These results are in agreement with Eqs. 5.3 and 5.4.

5.3 Approximate Assymptotic Solution For Initially Uniform Density

Equation 5.14 suggests that a suitable form for the density distribution as $t \to \infty$ for an initially uniform gas cloud is

$$\rho t^{j+1} = D\left(1-\eta^2\right)^{B} \qquad 5.16$$

where D and B are constants and $\eta = \frac{r}{R(t)}$.

Since the gas cloud is initially uniform

$$R = \frac{2}{\gamma - 1} t \qquad 5.17$$

The constants B and D can be determined from the conservation of mass and energy of the expanding cloud.

$$\frac{1}{j+1} = R^{j+1} \int_0^1 \rho \eta^j d\eta \qquad 5.18$$

$$\frac{1}{\gamma(\gamma-1)(j+1)} = R^{j+1} \int_0^1 \rho \frac{u^2}{2} \eta^j d\eta \qquad 5.19$$

Eq. 5.18 equates the mass at t = 0 to the mass at $t \rightarrow \infty$ and Eq. 5.19 equates the internal energy at t = 0 to the kinetic energy at $t \rightarrow \infty$ (the internal energy $\rightarrow 0$ as $t \rightarrow \infty$). Substituting Eqs. 5.16 and 5.17 into Eqs. 5.18 and 5.19 with $u = \frac{r}{t}$ yields

$$B = \frac{j+1}{2}\left(\frac{\gamma+1}{\gamma-1}\right) - 1 \qquad 5.20$$

and $$D = \frac{2}{j+1}\left(\frac{\gamma-1}{2}\right)^{j+1} \frac{\Gamma\{B+1+[(j+1)/2]\}}{\Gamma(B+1)\,\Gamma[(j+1)/2]} \qquad 5.21$$

Thus Eqs. 5.15, 5.16, 5.20 and 5.21 yield a solution for the expansion of an initially uniform gas cloud which assymptotically approaches the exact solution as $t \to \infty$.

6. FINITE DIFFERENCE SOLUTION OF REAL GAS EXPANSION

6.1 Basic Equations

The finite difference method of solution of a gas expanding into a vacuum is developed in order to be able to handle problems in which the equation of state is not of the perfect gas form. The equations of conservation of mass and momentum are written as in Section 2.1:

$$\frac{\partial \rho}{\partial t} + \rho \frac{\partial u}{\partial r} + u \frac{\partial \rho}{\partial r} + j \frac{\rho u}{r} = 0 \qquad 6.1$$

$$\frac{\partial u}{\partial t} + u \frac{\partial u}{\partial r} + \frac{a^2}{\rho} \frac{\partial \rho}{\partial r} = 0 \qquad 6.2$$

6.2 Equations of State

The equations of state used for the non-perfect gas solution are those empirically determined by Tillotson [5].

$$\bar{p} = \left\{ a + \frac{b}{\frac{\bar{E}}{\bar{E}_0 \eta^2} + 1} \right\} \bar{E} \bar{\rho} + \bar{A} \mu + \bar{B} \mu^2 \qquad 6.3$$

for compressed states, where a, b, $\bar{A}$ and $\bar{B}$ are constants for a given metal, and

$$\eta = \bar{\rho} / \bar{\rho}_0$$

$$\mu = \eta - 1 .$$

For the expansion of a shocked metal at low densities ($\bar{\rho}/\bar{\rho}_0 < 1$) the material behaves as a gas at these low densities if the internal energy $\bar{E}$ is greater than $\bar{E}_g$ the energy at which condensation begins. The behaviour is described by:

$$\bar{p} = a\bar{E}\bar{\rho} + \left\{ \frac{b\bar{E}\bar{\rho}}{\frac{\bar{E}}{\bar{E}_0\eta^2}+1} + \bar{A}\mu e^{-\beta\left(\frac{\bar{\rho}_0}{\bar{\rho}}-1\right)} \right\} e^{-\alpha\left(\frac{\bar{\rho}_0}{\bar{\rho}}-1\right)^2} \qquad 6.4$$

where a, b, and $\bar{A}$ are the same constants as in Eq. 6.3 and α and β are two additional constants for the metal considered. For very low densities (and if $\bar{E}$ is still greater than $\bar{E}_g$), $\left(\frac{\bar{\rho}_0}{\bar{\rho}}-1\right)^2 \gg 1$, and Eq. 6.4 reduces to the perfect gas relation

$$\bar{p} = a\bar{E}\bar{\rho} \qquad 6.5$$

If the internal energy $\bar{E}$ drops below the critical value $\bar{E}_g$, the material is assumed to partially condense and the condensed equation of state (Eq. 6.3) is used.

6.3 Calculation Of The Shocked Metal State

The Hugoniot relation across the shock is written as:

$$\bar{E}_s - \bar{E}_0 = \frac{1}{2}\left(\bar{p}_s + \bar{p}_0\right)\left(\frac{1}{\bar{\rho}_0} - \frac{1}{\bar{\rho}_s}\right) \qquad 6.6$$

The condensed equation of state (Eq. 6.3) and the Hugoniot relation (Eq. 6.6) can both be expressed in the form:

$$\bar{p} = f_1(\bar{\rho}, \bar{E}) \qquad 6.7$$

$$\bar{p} = f_2(\bar{\rho}, \bar{E}) \qquad 6.3$$

Once the shock strength is specified (by the density ratio $\frac{\bar{\rho}_s}{\rho_0}$), Eqs. 6.7 and 6.3 can be solved by Newton - Raphson iteration to yield the shocked state pressure and internal energy.

6.4 Isentropic Expansion of Shocked State

The isentropic relation (Eq. 2.5) is now used to obtain the isentrope for the expansion process.

$$\int_{\bar{E}_s}^{\bar{E}} d\bar{E} = \int_{\bar{\rho}_s}^{\bar{\rho}} \frac{\bar{p}}{\bar{\rho}^2}\, d\bar{\rho} \qquad 6.9$$

If the properties behind the shock are known ($\bar{\rho}_s$, $\bar{p}_s$, $\bar{E}_s$) and a small increment - $d\bar{\rho}$ is taken, Eq. 6.9 can be written in finite difference form

$$\bar{E} - \bar{E}_s = \frac{\bar{p}_{av}}{\bar{\rho}_{av}^2}\left(\bar{\rho} - \bar{\rho}_s\right) \qquad 6.10$$

where $\bar{p}_{av}$ is the average value of $\bar{p}$ over the interval and $\bar{\rho}_{av}$ is the average value of $\bar{\rho}$ over the interval. In general, between points n and $(n+1)$, assuming that the state is known at n,

$$\bar{\rho}_{n+1} = \bar{\rho}_n - d\bar{\rho} \qquad 6.11$$

$$\bar{E}_{n+1} = \bar{E}_n + \frac{\bar{p}_n}{\bar{\rho}_n^2}\left(\bar{\rho}_{n+1} - \bar{\rho}_n\right) \qquad 6.12$$

$\bar{p}_{n+1}$ can now be determined from $\bar{E}_{n+1}$ (first approximation) and $\bar{\rho}_{n+1}$ using the equation of state appropriate to the value of $\bar{\rho}_{n+1} / \bar{\rho}_0$.

Now, $$\bar{\rho}_{av} = \frac{\bar{\rho}_n + \bar{\rho}_{n+1}}{2} \qquad 6.13$$

$$\bar{p}_{av} = \frac{\bar{p}_n + \bar{p}_{n+1}}{2} \qquad 6.14$$

A second approximation for $\bar{E}_{n+1}$ is obtained from

$$\bar{E}_{n+1} = \bar{E}_n + \frac{\bar{p}_{av}}{\bar{\rho}_{av}^2}\left(\bar{\rho}_{n+1} - \bar{\rho}_n\right) \qquad 6.15$$

A new value of $\bar{p}_{n+1}$ is calculated from the equation of state appropriate to the value of $\bar{\rho}_{n+1} / \bar{\rho}_0$ (Eq. 6.3 if $\bar{\rho}_{n+1} / \bar{\rho}_0 > 1$; Eq. 6.4 if $\bar{\rho}_{n+1} / \bar{\rho}_0 < 1$). Any desired number of approximations may be taken by going back to

the relations 6.13, 6.14 and 6.15. As soon as $\bar{E}_{n+1}$ has reached a value equal to or less than $\bar{E}_g$ (the critical energy for condensation to begin), Eq. 6.4 is used as the equation of state.

If the initial shock strength is great enough, the perfect gas relation (Eq. 6.5) adequately describes the expanded state at low density before the internal energy $\bar{E}$ is reached the critical values $\bar{E}_g$, and the condensed equation of state (Eq. 6.3) is not used. This critical value of density is taken such that the exponent in Eq. 6.4 becomes

$$\alpha \left(\frac{\bar{\rho}_o}{\bar{\rho}_c} - 1 \right)^2 = 85$$

ie.
$$\bar{\rho}_c = \frac{\bar{\rho}_o}{1 + \sqrt{\frac{85}{\alpha}}} \qquad 6.16$$

If this value of density $\bar{\rho}_c$ is reached before $\bar{E}$ is less than $\bar{E}_g$, Eq. 6.5 becomes the equation of state of the metal, and the relation

$$\frac{\bar{P}}{\bar{\rho}^{\gamma}} = \frac{\bar{P}_c}{\bar{\rho}_c^{\gamma}} \qquad 6.17$$

is used to describe the further expansion of the gas, where $\gamma = (1+\alpha)$.

The values of $\bar{p}$ and $\bar{\rho}$ are retained at each value of $\bar{\rho}$ used to calculate the isentrope, and the isentrope is curve-fitted with a sixth-degree polynomial in the non-dimensional form

$$\frac{\bar{p}}{\bar{p}_s} = C_1 + C_2\left(\frac{\bar{\rho}}{\bar{\rho}_s}\right) + C_3\left(\frac{\bar{\rho}}{\bar{\rho}_s}\right)^2 + \ldots + C_7\left(\frac{\bar{\rho}}{\bar{\rho}_s}\right)^6 \qquad 6.18$$

The speed of sound at each point on the isentrope is found by calculating the slope of the $\bar{p}$, $\bar{\rho}$ isentrope between the two adjacent points.

$$\bar{a}_n = \sqrt{\left(\frac{\partial \bar{p}_n}{\partial \bar{\rho}_n}\right)_s} \qquad 6.19$$

where $$\frac{\partial \bar{p}_n}{\partial \bar{\rho}_n} = \frac{\bar{p}_{n+1} - \bar{p}_n}{\bar{\rho}_{n+1} - \bar{\rho}_n} \qquad 6.20$$

The speed of sound is also curve fitted with a sixth-degree polynomial in the non-dimensional form

$$\frac{\bar{a}}{\bar{a}_s} = d_1 + d_2\left(\frac{\bar{\rho}}{\bar{\rho}_s}\right) + d_3\left(\frac{\bar{\rho}}{\bar{\rho}_s}\right)^2 + \ldots + d_7\left(\frac{\bar{\rho}}{\bar{\rho}_s}\right)^6 \qquad 6.21$$

In the event that Eq. 6.17 is used to describe part of the isentrope, the curve fits are used only over the range $\bar{\rho}_c \leq \bar{\rho} \leq \bar{\rho}_s$ and the perfect gas relations are used over the range $0 \leq \bar{\rho} \leq \bar{\rho}_c$.

6.5 Boundary Conditions

The boundary conditions at the expansion and the escape fronts are:

Expansion Front:

$$\left.\begin{aligned} \tau_{ex} &= 1 - t \\ u_{ex} &= 0 \\ a_{ex} &= 1 \\ \rho_{ex} &= 1 \\ p_{ex} &= \bar{p}_s / \bar{\rho}_s \bar{a}_s^2 \end{aligned}\right\} \qquad 6.22$$

Escape Front:

$$\left.\begin{aligned} \tau_{es} &= 1 + u_f t \\ \text{where} \quad u_f &= \int_{\rho_{es}}^{1} a \frac{d\rho}{\rho} \\ a_{es} &= 0 \\ \rho_{es} &= \rho_{es} \\ p_{es} &= 0 \\ a_{es} &= 0 \end{aligned}\right\} \qquad 6.23$$

For a sufficiently strongly shocked metal, $\rho_{as} = 0$, but it is possible that the pressure of the metal becomes negative (ie. metal fails in tension) so that the pressure becomes zero at a finite density particular to the calculated isentrope.

6.6 Starting Conditions For Non-Perfect Gas

As in the case of the perfect gas (Section 4.5), the starting conditions are found by integration along a λ_1 and λ_2 characteristic.

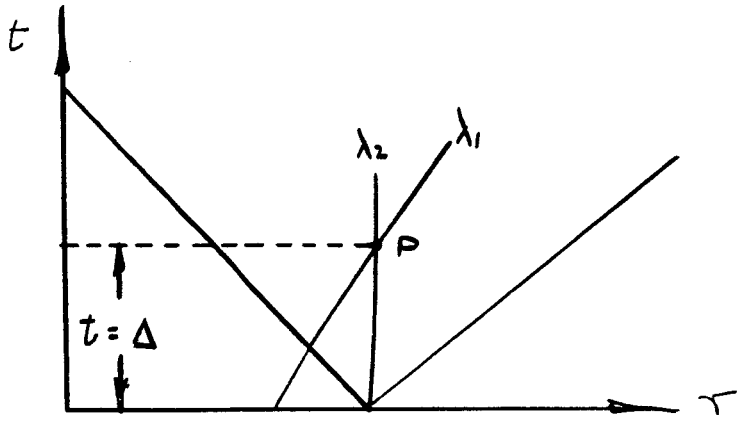

Fig. 6.1

Along λ_2 ,
$$\int_1^{\tau} d\tau = \int_0^{\Delta} (u - a)\, dt$$

ie.
$$\frac{\tau - 1}{\Delta} = u - a \qquad 6.24$$

Along λ_1, $\int_0^u du = -\int_1^\rho a \frac{d\rho}{\rho} = \int_\rho^1 a \frac{d\rho}{\rho}$

ie. $$u = \int_\rho^1 a \frac{d\rho}{\rho} \qquad 6.25$$

From Eqs. 6.24 and 6.25

$$\frac{\gamma - 1}{\Delta} = \int_\rho^1 a \frac{d\rho}{\rho} - a \qquad 6.26$$

In order to obtain the starting distributions of ρ and u at t = Δ, the integral in Eq. 6.26 is evaluated for a number of values of ρ.

$$\int_\rho^1 a \frac{d\rho}{\rho} = \int_{\bar\rho/\bar\rho_s}^1 \frac{\bar a}{\bar a_s} \frac{d\left(\frac{\bar\rho}{\bar\rho_s}\right)}{\frac{\bar\rho}{\bar\rho_s}} \qquad 6.27$$

Carrying out the integration of Eq. 6.27 with Eq. 6.21

$$\int_\rho^1 a \frac{d\rho}{\rho} = \left[d_2 + \frac{d_3}{2} + \frac{d_4}{3} + \ldots + \frac{d_7}{6}\right] - \left[d_1 \ln\rho + d_2\rho + \frac{d_3}{2}\rho^2 + \ldots + \frac{d_7}{6}\rho^6\right] \qquad 6.28$$

Since $a = \frac{\bar a}{\bar a_s}$ is known (Eq. 6.21), $\frac{\gamma - 1}{\Delta}$ can be evaluated for any value of ρ ($0 \leq \rho \leq 1$).

In the event that Eq. 6.17 partly describes the isentropic expansion of the gas, Eq. 6.21 is used only over the range $\bar\rho_c \leq \bar\rho \leq \bar\rho_s$, and the perfect gas

relation (Eq. 6.17) is used over the range $0 \leq \bar{\rho} \leq \bar{\rho}_c$.

The density can now be expressed in the form

$$\rho = g_1 + g_2\left(\frac{r-1}{\Delta}\right) + g_3\left(\frac{r-1}{\Delta}\right)^2 + \ldots + g_7\left(\frac{r-1}{\Delta}\right)^6 \qquad 6.29$$

and u can be evaluated from Eqs. 6.23 and 6.28.

At the expansion front, $r = 1 - \Delta$ and $\rho_{ex} = 1$

From Eq. 6.26

$$a_{ex} = 1$$

and from Eq. 6.25

$$u_{ex} = 0$$

At the escape front $r = 1 + u_f t = 1 + \Delta \int_{\rho_{es}}^{1} a \frac{d\rho}{\rho}$ and

$$\rho = \rho_{es}$$

From Eq. 6.26

$$a_{es} = 0$$

From Eq. 6.25

$$u_{es} = \int_{\rho_{es}}^{1} a \frac{d\rho}{\rho} = u_f$$

The starting conditions (Eqs. 6.25 and 6.26) thus satisfy the boundary conditions (Eqs. 6.22 and 6.23) at both the expansion and the escape fronts.

6.7 Continuation of Solution

The solution for time greater than Δ is carried on in the same manner as for the perfect gas

(Section 4.2) except that the finite difference equations are written in the variables ρ and u.

From Eqs. 2.10 and 2.11

$$\frac{\partial \rho}{\partial t} = -\rho \frac{\partial u}{\partial r} - u \frac{\partial \rho}{\partial r} - j \frac{\rho u}{r} \qquad 6.30$$

$$\frac{\partial u}{\partial t} = -u \frac{\partial u}{\partial r} - \frac{a^2}{\rho} \frac{\partial \rho}{\partial r} \qquad 6.31$$

The numerical derivatives are:

$$\frac{\partial}{\partial r} u(r,t) = \frac{u(r+\Delta r, t) - u(r-\Delta r, t)}{2\Delta r} \qquad 6.32$$

$$\frac{\partial}{\partial r} \rho(r,t) = \frac{\rho(r+\Delta r, t) - \rho(r-\Delta r, t)}{2\Delta r} \qquad 6.33$$

$$u(r, t+\Delta t) = \Delta t \frac{\partial}{\partial t} u(r,t) + \frac{1}{2}\left[u(r-\Delta r, t) + u(r+\Delta r, t)\right] \qquad 6.34$$

$$\rho(r, t-\Delta t) = \Delta t \frac{\partial}{\partial t} \rho(r,t) + \frac{1}{2}\left[\rho(r-\Delta r, t) + \rho(r+\Delta r, t)\right] \qquad 6.35$$

Using Eqs. 6.30 to 6.35, the solution may be carried out identically as in Section 4.2. A slight difference arises when the center is reached.

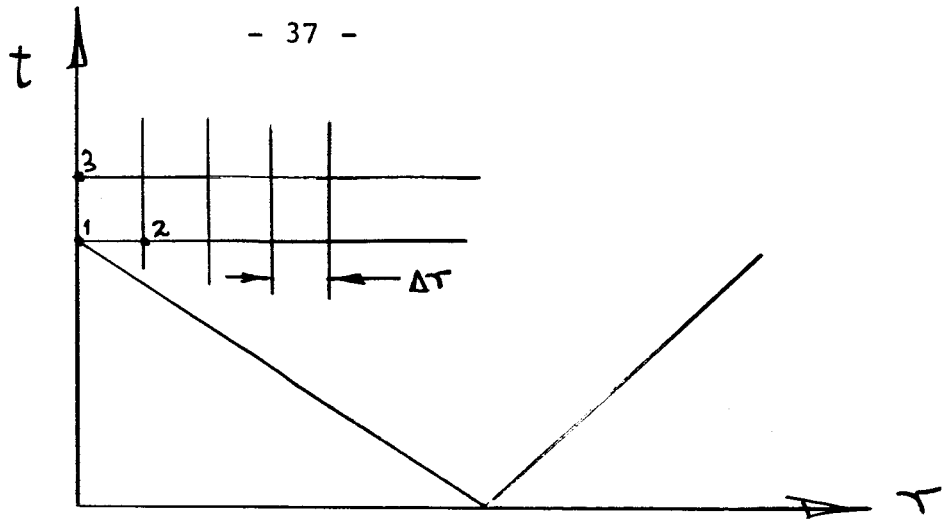

Fig. 6.2

At the center

$$u(\Delta r, t) = -u(-\Delta r, t) \qquad 6.36$$

$$\rho(\Delta r, t) = \rho(-\Delta r, t) \qquad 6.37$$

$$\frac{\partial u}{\partial r}\Big|_{r=0} = \frac{u(\Delta r, t)}{\Delta r} \qquad 6.38$$

$$\frac{\partial \rho}{\partial r}\Big|_{r=0} = 0 \qquad 6.39$$

The term $j\frac{\rho u}{r}$ in Eq. 6.30 has a limit at r=0.

$$\lim_{r\to 0} j\frac{\rho u}{r} = \lim_{r\to 0} j\frac{\frac{\partial}{\partial r}(\rho u)}{\frac{\partial}{\partial r}(r)} = j\frac{\rho u(\Delta r)}{\Delta r} \qquad 6.40$$

Refering to Fig. 6.2

$$\frac{\partial u}{\partial r}\Big|_1 = \frac{u(2)}{\Delta r}$$

$$\left.\frac{\partial \rho}{\partial r}\right|_1 = 0$$

$$\lim_{r \to 0} j \frac{\rho u}{r} = j \frac{\rho(1) u(2)}{\Delta r}$$

The procedure is then basically the same as in Section 4.2.

7. DETAILED NUMERICAL PROCEDURES

7.1 Solution By Method of Characteristics

The origin of the expansion is assumed to be at the point (1,0) in the r,t diagram (Fig. 7.1).

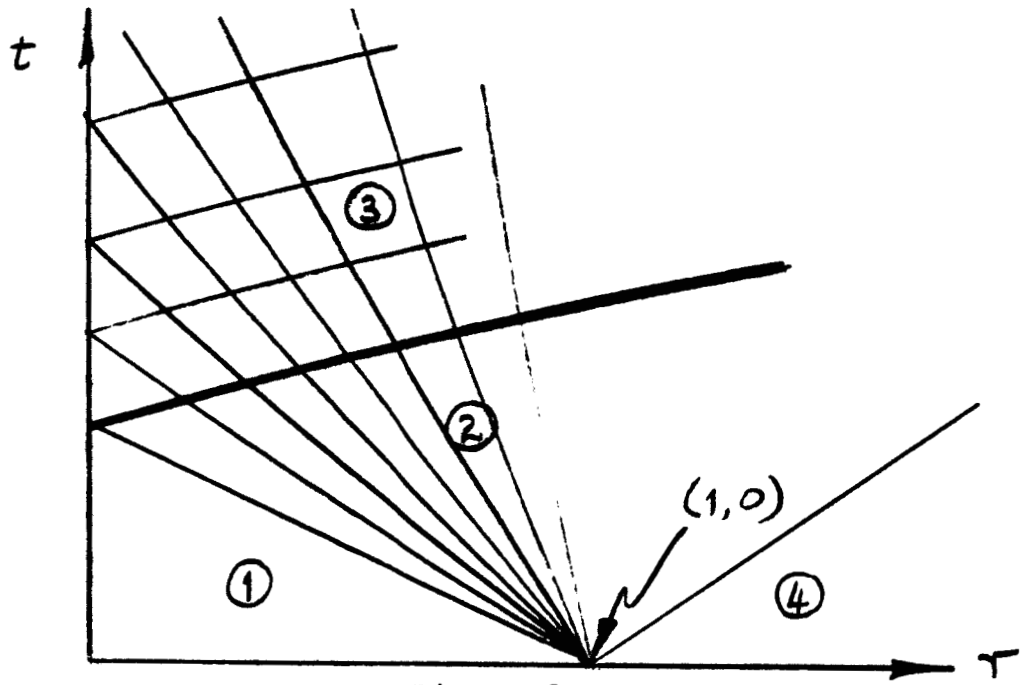

Fig. 7.1

The r,t plane can be divided into four distinct regions, the region of undisturbed gas (Region 1) the centered wave region (Region 2), the reflected wave region (Region 3) and the vacuum ahead of the escape front (Region 4). The conditions at the fronts proceeding into regions 1 and 4 are known:

$$\left.\begin{aligned} u_1 &= 0 \\ a_1 &= \bar{a}_1/\bar{a}_s = 1 \\ \rho_1 &= \bar{\rho}_1/\bar{\rho}_s = 1 \\ p_1 &= \bar{p}_1/\bar{\rho}_s\bar{a}_s^2 = \bar{p}_s/\bar{\rho}_s\bar{a}_s^2 \end{aligned}\right\} \qquad 7.1$$

$$\left.\begin{aligned} u_4 &= u_{es} \\ a_4 &= 0 \\ \rho_4 &= 0 \\ p_4 &= 0 \end{aligned}\right\} \qquad 7.2$$

a) Starting the Solution

In order to begin the solution, consider a centered expansion at r = 1, t = 0.

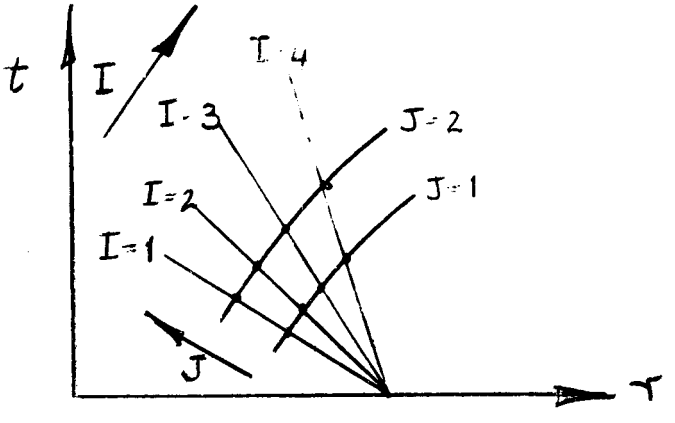

Fig. 7.2

Co-ordinates in the r - t plane are now referred to as $r(i,j)$, $t(i,j)$ where the subscripts i and j take values as indicated in Fig. 7.2. The properties at the head of the rarefaction fan are known:

$$\left.\begin{aligned} u(1,1) &= 0 \\ a(1,1) &= 1 \\ \rho(1,1) &= 1 \\ p(1,1) &= \bar{p}_s / \bar{\rho}_s \bar{a}_s^2 \end{aligned}\right\} \qquad 7.3$$

Taking r(1, 1) = 0.99,

$$p(2,1) = p(1,1) + \Delta p \qquad 7.4$$

and assuming one-dimensional flow from the origin of the expansion to the characteristic line j = 1, the velocity u(2,1) is determined from Eq. 3.2 in finite difference form

$$u(2,1) = u(1,1) - \frac{\Delta p}{\rho(1+\frac{1}{2},1)\,a(1+\frac{1}{2},1)} \qquad 7.5$$

where the subscript (1 + 1/2, 1) denotes the average value of a property between (1, 1) and (2, 1),

$$\rho(1+\tfrac{1}{2},1) = \frac{\rho(1,1) + \rho(2,1)}{2} \qquad 7.6$$

$$a(1+\tfrac{1}{2},1) = \frac{a(1,1) + a(2,1)}{2} \qquad 7.7$$

Both ρ(2, 1) and a(2, 1) are determined from the isentropic relations (Eq. 3.5 and 3.6), since p(2,1) is known. The propagation velocity of the right-running wave is (from Eq. 3.1)

$$c_R = u(1+\tfrac{1}{2},1) + a(1+\tfrac{1}{2},1)$$

$$c_R = \frac{1}{2}\left[u(1,1) + a(1,1) + u(2,1) + a(2,1)\right] \qquad 7.8$$

The propagation velocity of the left-running wave is (from Eq. 3.3).

$$c_L = u(2,1) - a(2,1) \qquad 7.9$$

The intersection point of the two waves in the r, t plane is found by writing Eqs. 3.1 and 3.3 in finite difference form

$$\left.\begin{aligned} \lambda_1 &: \quad r(2,1) - r(1,1) = c_R \left[t(2,1) - t(1,1) \right] \\ \lambda_2 &: \quad r(2,1) - 1 = c_L \left[t(2,1) - 0 \right] \end{aligned}\right\} \qquad 7.10$$

Eqs. 7.10 are solved to yield:

$$\left.\begin{aligned} t(2,1) &= \left[c_R\, t(1,1) - r(1,1) + 1 \right] \Big/ \left[c_R - c_L \right] \\ r(2,1) &= c_R \left[t(2,1) - t(1,1) \right] + r(1,1) \end{aligned}\right\} \qquad 7.11$$

The intersection point r(2, 1), t(2, 1) is thus determined. To determine the remaining points along the line j = 1, the general relations are:

$$p(i,1) = p(i-1,1) + \Delta p \qquad 7.12$$

$a(i, 1)$ and $\rho(i, 1)$ are found from Eqs. 3.5 and 3.6.

$$u(i,1) = u(i-1,1) - \frac{\Delta p}{\rho(i+\frac{1}{2},1)\, a(i+\frac{1}{2},1)} \qquad 7.13$$

The intersection point r(i, 1), t(i, 1) is given by:

$$\left.\begin{aligned} t(i,1) &= \left[C_R\, t(i-1,1) - \tau(i-1,1) + 1\right] \Big/ \left[C_R - C_L\right] \\ \tau(i,1) &= C_R \left[t(i,1) - t(i-1,1)\right] + \tau(i-1,1) \end{aligned}\right\} \qquad 7.14$$

where $$C_R = \frac{1}{2}\left[u(i-1,1) + a(i-1,1) + u(i,1) + a(i,1)\right] \qquad 7.15$$

and $$C_L = u(i,1) - a(i,1) \qquad 7.16$$

b) <u>Solution in Centered Wave Region</u>

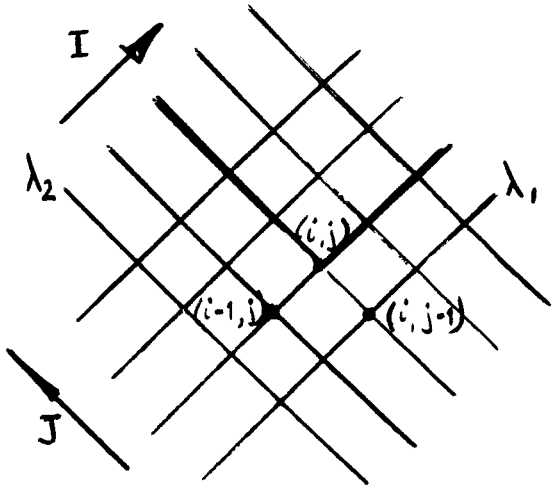

Fig. 7.3a

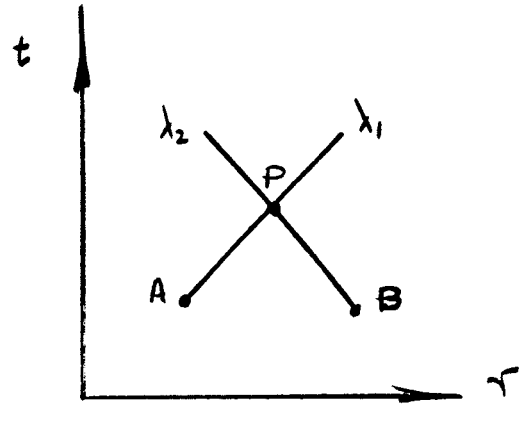

Fig. 7.3b

The point (i, j) is to be determined from the known properties at the points (i - 1, j) and (i, j - 1) in Fig. 7.3a.

Assuming that the grid points are sufficiently close together that the dependent variables vary linearly between adjacent points. Eqs. 3.1 to 3.4 may be written in finite difference forms (Eqs. 3.7 to 3.10).

Since the values of the properties at points A and B (Fig. 7.3b) are known, one may write as a first approximation:

$$\left.\begin{aligned}
(u+a)_{\lambda_1} &= u_A + a_A \\
(u-a)_{\lambda_2} &= u_B - a_B \\
(\rho a)_{\lambda_1} &= \rho_A a_A \\
(\rho a)_{\lambda_2} &= \rho_B a_B \\
(\rho a)_1 j \left(\frac{au}{r}\right)_{\lambda_1} &= \rho_A a_1 j \frac{a_A u_A}{r_A} \\
(\rho a)_{\lambda_2} j \left(\frac{au}{r}\right)_{\lambda_2} &= \rho_B a_B j \frac{a_B u_B}{r_B}
\end{aligned}\right\} \quad 7.17$$

Values for t_p, r_p, u_p and p_p can now be determined from Eqs. 3.11 to 3.14, and both ρ_p and a_p are found from Eqs. 3.5 and 3.6.

A second approximation for the properties at point P is found using the first calculated values at P, and putting:

$$
\left.
\begin{aligned}
(u+a)_{\lambda_1} &= \tfrac{1}{2}\left(u_A + a_A + u_P + a_P\right) \\
(u-a)_{\lambda_2} &= \tfrac{1}{2}\left(u_B - a_B + u_P - a_P\right) \\
(\rho a)_{\lambda_1} &= \tfrac{1}{2}\left(\rho_A a_A + \rho_P a_P\right) \\
(\rho a)_{\lambda_2} &= \tfrac{1}{2}\left(\rho_B a_B + \rho_P a_P\right) \\
(\rho a)_{\lambda_1} j\left(\frac{au}{r}\right)_{\lambda_1} &= \frac{1}{2}\left(\rho_A a_A j \frac{a_A u_A}{r_A} + \rho_P a_P j \frac{a_P u_P}{r_P}\right) \\
(\rho a)_{\lambda_2} j\left(\frac{au}{r}\right)_{\lambda_2} &= \frac{1}{2}\left(\rho_B a_B j \frac{a_B u_B}{r_B} + \rho_P a_P j \frac{a_P u_P}{r_P}\right)
\end{aligned}
\right\} \quad 7.18
$$

These values are now put into Eqs. 3.11 to 3.14, and more accurate values for the properties at point P are calculated. Any point in the centered wave region can be determined in this way provided that the previous point on both the right - and left-running characteristic lines are known.

c) Treatment At The Center

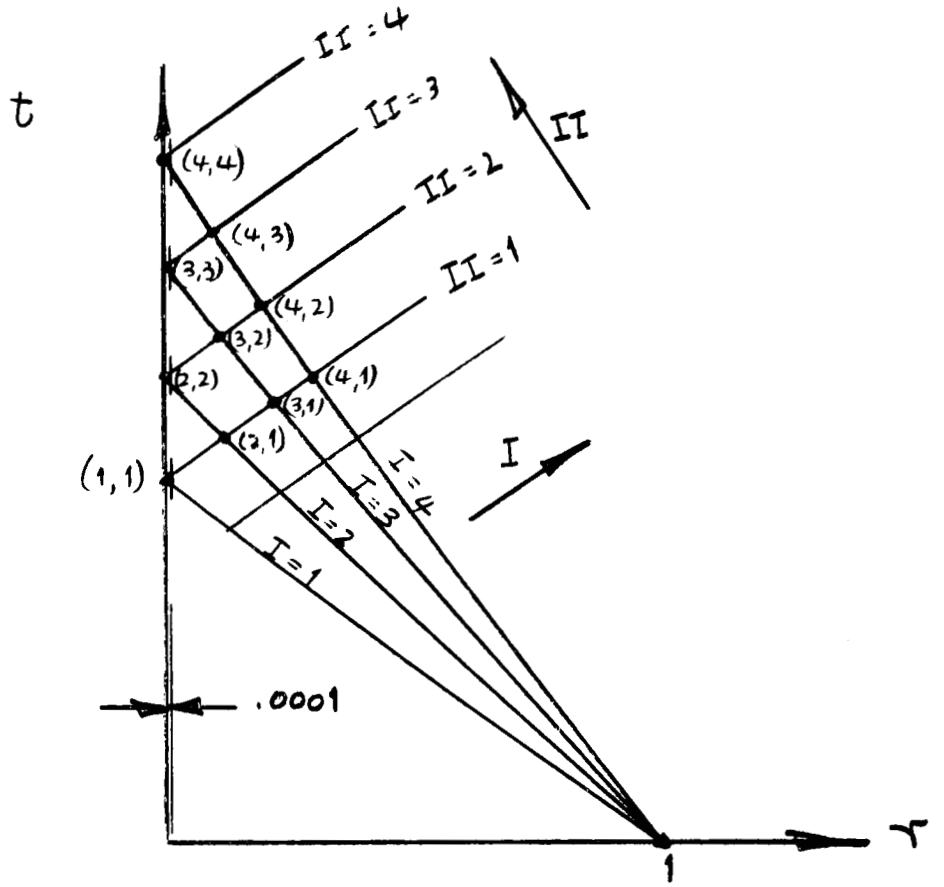

Fig. 7.4

In order to avoid the singularity of the term $\int \frac{\partial u}{\tau}$ in Eqs. 3.2 and 3.4, a slender rod of 0.0001 times the radius of the origin of the expansion is placed in the flow field. Points are now subscripted r(I, II), t(I, II).

At the center point (1, 1) in Fig. 7.4,

$$\left.\begin{aligned} \tau(1,1) &= .0001 \\ t(1,1) &= 1.0 \\ u(1,1) &= 0. \end{aligned}\right\} \qquad 7.19$$

$$\left.\begin{aligned} a(1,1) &= 1 \\ \rho(1,1) &= 1 \\ p(1,1) &= \bar{p}_s / \bar{\rho}_s \bar{a}_s^2 \end{aligned}\right]$$

The points (2, 1), (3, 1).....etc. are found as outlined in Section 7.1.b.

The first approximation for the point (2, 2) in Fig. 7.4 is found as follows:

$$\left.\begin{aligned} (u-a)_{\lambda_2} &= u(2,1) - a(2,1) \\ (\rho a)_{\lambda_2} &= \rho(2,1)\, a(2,1) \\ (\rho a)_{\lambda_2} j \left(\frac{\partial u}{\tau}\right)_{\lambda_2} &= \rho(2,1)\, a(2,1)\, j \frac{a(2,1)\, u(2,1)}{\tau(2,1)} \end{aligned}\right\} \quad 7.20$$

Using Eqs. 3.9, 3.10 and 7.20, and the conditions that

$$\left.\begin{aligned} u(2,2) &= 0 \\ \tau(2,2) &= 0.0001 \end{aligned}\right\} \quad 7.21$$

one obtains $$t(2,2) = t(2,1) + \frac{\tau(2,2) - \tau(2,1)}{u(2,1) - a(2,1)} \quad 7.22$$

$$p(2,2) = -\rho(2,1)\,a(2,1)\,u(2,1) + p(2,1)$$

$$-\rho(2,1)\,a(2,1)\,j\,\frac{a(2,1)\,u(2,1)}{\tau(2,1)}\left[t(2,2)-t(2,1)\right] \qquad 7.23$$

ρ(2, 2) and a(2, 2) are found from the isentropic relations (Eqs. 3.5 and 3.6)

The second approximation is taken as:

$$\left.\begin{aligned}
(u-a)_{\lambda_2} &= \frac{1}{2}\left[u(2,1) - a(2,1) - a(2,2)\right] \\
(\rho a)_{\lambda_2} &= \frac{1}{2}\left[\rho(2,1)\,a(2,1) + \rho(2,2)\,a(2,2)\right] \\
(\rho a)_{\lambda_2}\,j\left(\frac{au}{\tau}\right)_{\lambda_2} &= \frac{1}{2}\left[\rho(2,1)\,a(2,1)\,j\,\frac{a(2,1)\,u(2,1)}{\tau(2,1)}\right]
\end{aligned}\right\} \qquad 7.24$$

Again

u(2, 2) = 0.

r(2, 2) = 0.0001

New values are calculated for t(2,2) and p(2,2) using Eqs. 7.24, 3.9 and 3.10. The procedure of Section 7.1.b is

followed to obtain points (3,2), (4,2)...etc.

The properties at point (3,3) are found from those at point (3,2) in the same manner that the properties at (2,2) were determined from those at (2,1). The entire flow field of the reflected wave region can therefore be determined.

7.2 Numerical Procedure in Finite Difference Method

The basic procedure for the numerical solution of the expansion problem has been outlined in Sections 4.1 to 4.4. In this section, the method of construction of the grid is outlined and additional numerical interpolation formulae are introduced for use when the expansion or escape fronts do not pass through a grid point.

a) Construction of Grid

The velocities of both the expansion and the escape fronts are known. For a perfect gas

$$\left.\begin{aligned} \mu_{ex} &= 1 \\ \mu_f &= \frac{2}{\gamma - 1} \end{aligned}\right\} \qquad 7.1$$

For a non-perfect gas

$$\left.\begin{aligned} \mu_{ex} &= 1 \\ \mu_f &= \int_{\rho_{es}}^{1} a \frac{d\rho}{\rho} \end{aligned}\right\} \qquad 7.2$$

The increment Δr is chosen such that there are 501 grid points when the expansion front has reached the center (t = 1).

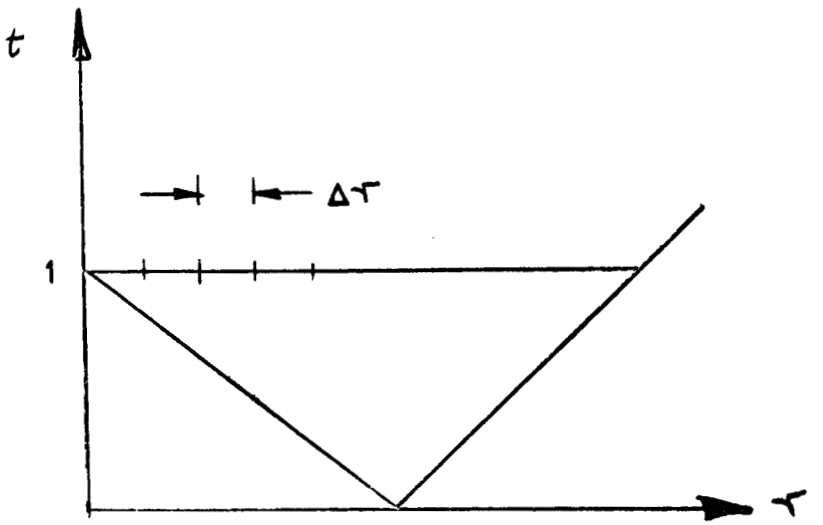

Fig. 7.5

This condition is expressed by

$$\Delta\tau = \frac{(1 + u_f)}{500} \qquad 7.3$$

A starting time Δ must now be chosen

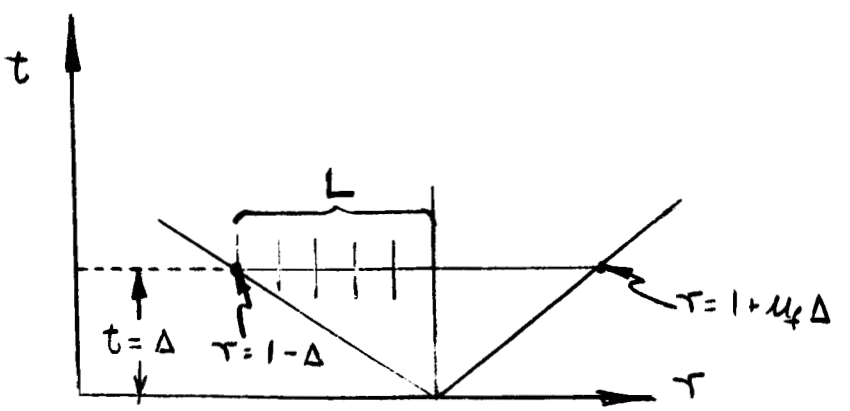

Fig. 7.6

Referring to Fig. 7.6 , Δ is chosen such that

$$L = 5\Delta r \qquad 7.4$$

Since $\mu_{ex} = 1$, it can be seen that $\Delta = 5\Delta r$ is the appropriate starting time for the solution. The right hand extremity of the grid is defined by:

$$r_{es} = 1 + \mu_f \Delta \qquad 7.5$$

and the left hand extremity by

$$r_{ex} = 1 - \Delta = 1 - 5\Delta r \qquad 7.6$$

The points on the grid between r = r_{es} and r = r_{ex} are defined by:

$$r_n = r_{n-1} + \Delta r \qquad 7.7$$

A condition for the stability of the solution by the finite difference method is that $\frac{\Delta r}{\Delta t} \geq$ greatest velocity in the system. In practice, it was found that a ratio $\frac{\Delta r}{\Delta t}$ of 4 yielded good results, and this ratio was used.

$$\Delta t = \frac{\Delta r}{4} \qquad 7.8$$

The time increment Δt is now defined, and the grid can be drawn for times greater than the starting time Δ . The two boundary conditions which are maintained are:

$$u_{ex} = 1 - t \qquad 7.9$$

$$u_{es} = 1 + u_f t \qquad 7.10$$

The grid size and location is maintained until the solution has reached time t = 1, and points are added to the grid where necessary until the number of points is 501 at t = 1.

Several additional interpolation techniques must be used so that the solution can be obtained when the expansion or escape fronts do not pass through a grid point. In all cases, the boundary conditions at both fronts are known.

b) Solution Near Escape Front

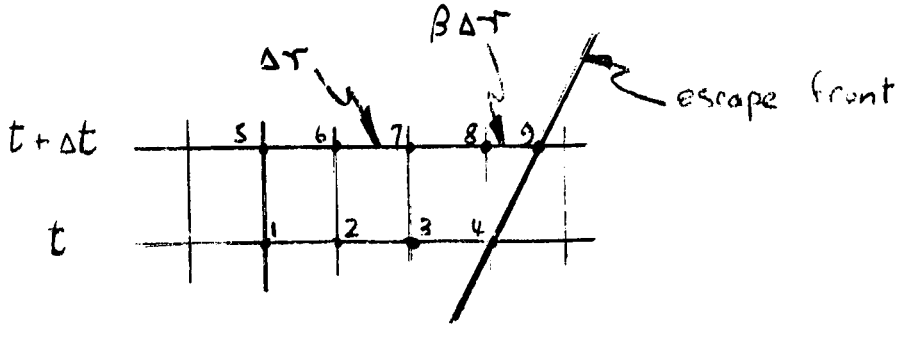

Fig. 7.7

The properties at points 1 to 4 have been determined, and it is desired to obtain the solution for points 5 to 9 at the next time $t = t + \Delta t$ (Fig. 7.7).

Points 5, 6 and 7 can be obtained by the method of Section 4.2 knowing the properties at points 1 to 4.

The distance between points 7 and 3 is Δr, and that between points 3 and 9 is $\beta \Delta r$. The properties at point 9 are known from the boundary conditions at the escape front, and the properties at 8 are determined by interpolation.

$$a(8) = \frac{a(9) + \beta a(7)}{1 + \beta}$$

$$u(8) = \frac{u(9) + \beta u(7)}{1 + \beta} \qquad 7.11$$

c) Solution Near Expansion Front

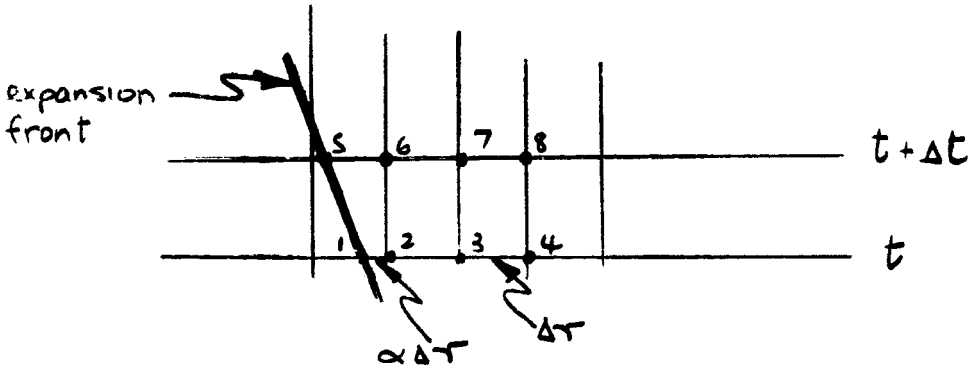

Fig. 7.8

If the situation in Fig. 7.9 arises, the properties at $t = t + \Delta t$ are found as follows:

The properties at points 1 to 4 are known, and those at point 5 are known from the boundary conditions at the expansion front. The properties at points 7, 8....can be found from those at points 2, 3, 4....as outlined in Section 4.2.

If the distance between points 1 and 2 is $\alpha \Delta\tau$ and that between points 2 and 3 is Δr, one may write:

$$\frac{\partial a}{\partial t}(2) = \frac{1}{\Delta t}\left\{a(6) - \frac{1}{3}\left[a(2) + \frac{2\alpha}{1+\alpha}a(3) + \frac{2}{1+\alpha}a(1)\right]\right\} \quad 7.12$$

$$\frac{\partial u}{\partial t}(2) = \frac{1}{\Delta t}\left\{u(6) - \frac{1}{3}\left[u(2) + \frac{2\alpha}{1+\alpha}u(3) + \frac{2}{1+\alpha}u(1)\right]\right\} \quad 7.13$$

$$\frac{\partial a}{\partial \tau}(2) = \frac{1}{3(1+\alpha)\Delta\tau}\left\{(3-\alpha)a(3) + (1+\alpha)a(2) - 4a(1)\right\} \quad 7.14$$

$$\frac{\partial u}{\partial \tau}(2) = \frac{1}{3(1+\alpha)\Delta\tau}\left\{(3-\alpha)u(3) + (1+\alpha)u(2) - 4u(1)\right\} \quad 7.15$$

Equations 7.12 to 7.15, along with Eqs. 4.3 and 4.4, can be used to find the properties at point 6.

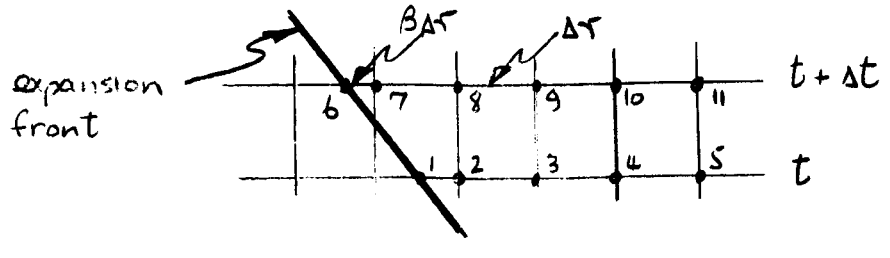

Fig. 7.9

If the wave intersection with the grid occurs as in Fig. 7.9, the following technique is used: Points 9, 10...etc. are determined from points 2, 3, 4, 5...etc. as in Section 4.2. The properties at point 3 are found from those at 1, 2, and 3 as outlined in this section above. The properties at point 6 are known from the boundary conditions at the expansion front, and the properties at point 7 are:

$$\left.\begin{aligned} a(7) &= \frac{\beta a(8) + a(6)}{1+\beta} \\ u(7) &= \frac{\beta u(8) + u(6)}{1+\beta} \end{aligned}\right\} \qquad 7.16$$

d) Continuation of Solution Beyond t = 1

Once the time t = 1 has been reached, the grid size is doubled (both Δ r and Δ t are doubled) and the number of points is reduced to 251.

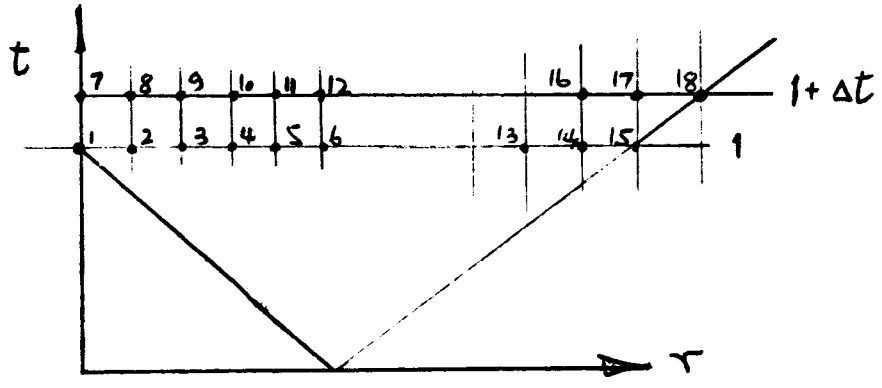

Fig. 7.10

Points 8, 9, 10... and point 16 (in Fig. 7.10) are found as in Section 4.2. The boundary condition at 13 is known, and the properties at 17 are found from those at 16 and 13. The point 7 is then determined by the method outlined in Section 4.4. The solution for the flow can thus be obtained for the time beyond t = 1.

8. RESULTS AND DISCUSSION

3.1 Finite Difference Solution For Cylindrical Expansion of Perfect Gas With $\gamma = 1.4$

The escape front velocity of a perfect gas is given by Eq. 4.12 and it is seen that for such a gas with a specific heat ratio of 1.4, the escape front velocity is five times the expansion front velocity.

The speed of sound profiles at times t = 0, 0.5, 1.0 and 2.0 are given in Fig. 8.1. It is seen that at time t = 0.5, the speed of sound distribution is almost a linear one, comparing closely to the distribution for the corresponding distribution for the plane case (see Section 8.2). The term in the continuity equation (Eq. 4.1) which causes the departure from linearity in the cylindrical expansion is $\frac{1}{r}\frac{\partial u}{\partial r}$ (for the cylindrical case, $\frac{1}{r} = 1$), but at this relatively short time from the initiation of the expansion, the expansion front has advanced only to half the original radius and this term is small. The escape front velocity, as pointed out above, is five times that of the expansion front, and this front has proceeded out to a radius of 3.5, where the boundary condition of a = 0 applies. At t = 1.0, the head of the expansion wave has reached the center and

the fluid states at r = 0 begin to decay. The escape front position is now r = 6, where the boundary condition (a = 0) applies. The non-linearity of the speed of sound distribution is now more apparent due to the increased effect of the term $\lambda \frac{au}{r}$. At t = 2, the expansion front has been reflected from the center (of the cylinder), and has caused a further decay in the speed of sound to the radius to which the reflection has penetrated (approximately 2.0). The speed of sound is approximately constant (a = .625) from the center to r = 1.5.

The corresponding density profiles for the cylindrical expansion at times t = 0, 0.5, 1.0 and 2.0 are shown in Fig. 8.2. The decay in density is more rapid than the speed of sound decay, since from the isentropic relations (Eqs. 2.6 and 2.7), it can be seen that the density varies as the speed of sound raised to the power $\frac{2}{\gamma - 1}$, or 5 for the case of a specific heat ratio of 1.4. The density variation is otherwise analogous to the speed of sound variation.

The velocity distributions at times t=0.5, 1.0 and 2.0 are plotted in Fig. 8.3. At t = .5, the distribution is approximately linear, varying from 0 at r = .5 (boundary condition at the expansion front) to 5 at r = 3.5 (boundary condition at the escape front). Again, as in the

case of the speed of sound distribution, the velocity profile becomes increasingly non-linear as time increases, with the boundary conditions of zero velocity at the center, and a velocity of 5 at the escape front maintained.

8.2. Comparison of Finite Difference Solutions of Plane, Cylindrical and Spherical Expansions for Perfect Gas With $\gamma = 1.4$

The speed of sound distribution at time t = 0.5 for the plane expansion is shown in Fig. 8.4, and it is seen to be a linear distribution from a = 1 at r = 0.5 to a = 0 at r = 3.5, the two boundary conditions which are imposed. The solution obtained by the finite difference method is therefore identical to the closed form of the solution which can be obtained for a plane expansion. Results at greater times indicate that the finite difference solution is correct for the plane case for times greater than t = 0.5.

A comparison of the results for the plane, cylindrical and spherical expansions for t = 0.5 is shown in Fig. 8.5. The boundary conditions are satisfied in each case at r = 0.5 and r = 3.5. The distribution for the plane case is linear as in Fig. 8.4 above. There is a slight non-linearity for the cylindrical solution, with

the decay being more rapid due to the term $j\frac{au}{r}$ in the continuity equation (Eq. 4.1). For the spherical case, this effect is most pronounced and the greatest departure from linearity is seen here. At time t = 1, the plane cylindrical and spherical solutions are again compared (Fig. 8.6), and the same qualitative behaviour is noted as in Fig. 8.5. It is seen that the speed of sound gradient $\frac{\partial a}{\partial r}$ is greater for the spherical case near r = 0 than it is for the cylincrical or plane solutions.

A comparison of the speed of sound distributions for the plane and cylindrical expansion at t = 1.5 is shown in Fig. 8.7. For the plane case, the value of "a" at the center is 0.879, and for the cylindrical case, the value is 0.733. The more rapid decay at the center for the cylindrical case is due to the sharper gradient of "a" ($\frac{\partial a}{\partial r}$) near the center, and the effect of the term $j\frac{au}{r}$ on the time derivative $\frac{\partial a}{\partial t}$ (Eq. 4.3).

8.3. Comparison of Cylindrical Expansions of Perfect Gases With $\gamma = 3.0$ and $\gamma = 1.4$

It has been noted that a perfect gas description of metal states has served to predict the behaviour of the expansion process. Using the approximation of the limiting density ratio of a strong shock.

$$\sigma = \frac{\gamma + 1}{\gamma - 1} \qquad 8.1$$

For a shock strength $\sigma = 2$, the effective γ is 3.0. The perfect gas solution for $\gamma = 3.0$ is now obtained for later comparison to the real gas solution for $\sigma = 2.0$.

The speed of sound and velocity distributions as functions of r at t = 0.5 for the cylindrical case shown in Figs. 3.8 and 8.9. For the perfect gas with $\gamma = 3.0$, the escape front velocity is 1, the same as the expansion front velocity. The boundary condition (a = 0) at the escape front occurs at r = 2, as opposed to r = 3.5 for the perfect gas with $\gamma = 1.4$. As a result, the gradient of "a" with respect to "r" is sharper for this gas ($\gamma = 3.0$) than for the gas with $\gamma = 1.4$. The corresponding distributions for the gas with $\gamma = 1.4$ are shown in Figs. 8.3 and 8.9 for comparison and the sharper gradient ($\frac{\partial a}{\partial r}$) is apparent for the case of $\gamma = 3.0$.

The speed of sound distributions for both γ = 1.4 and γ = 3.0 at time t = 1.0 are shown in Fig. 8.10, and it is again apparent that the gradient $\frac{\partial a}{\partial r}$ is much greater for γ = 3.0 than it is for γ = 1.4. The effect of the sharper gradient for γ = 3.0 becomes apparent when the speed of sound distributions are plotted at time t = 2.0 for the two cases (Fig. 8.11). Where in the case of γ = 1.4, the value of "a" at the center is 0.625 at t = 2.0, "a" at the center is 0.231 for the case of γ = 3.0, at the same time. There is also a slight increase in "a" from r = 0 to r = 0.8.

8.4 Comparison of Characteristic Solution With Finite Difference Solution for Cylindrical Expansion of Perfect Gases

In order to check the solution of the expansion of a perfect gas of constant γ as obtained by the finite difference method solution of the same cases by the characteristic method (Secs. 3 and 7.1) was effected.

For the perfect gas with a specific heat ratio of 1.4, the speed of sound distribution at times t = 0.5, 1.0 and 2.0 are shown in Figs. 8.12 to 8.14. The solid line represents the characteristic solution, and the crosses represent points obtained by the finite difference method of solution. Extremely good agreement is noted,

especially for radii far away from the escape front. Near the escape front, slight discrepancy is noted for these cases and the reason shall be discussed in the next section.

The results for a perfect gas with $\gamma = 3.0$ are presented in Figs. 8.15 and 8.16. Again, the speed of sound distributions obtained by the characteristic method at times t = 0.5 and t = 2.0 are represented by the solid lines, and the crosses indicate points obtained by the finite difference method of solution. Here, agreement is extremely good, even in the region near the escape front.

8.5. Stability of the Finite Difference Solution

The stability of the finite difference method of solution (its resistance to oscillation) is dependent upon the grid size which is utilized in obtaining the solution. At the onset of this work, it was thought that the use of a grid ratio $\frac{\Delta r}{\Delta t}$ such that this ratio was equal to or greater than the maximum velocity in the expansion system was sufficient to ensure the stability of the solution obtained. The first results for the perfect gas with $\gamma = 3.0$ were obtained using a grid ratio $\frac{\Delta r}{\Delta t}$ equal to 1, the velocity of the expansion front and the escape front. The results obtained

are plotted as crosses in Fig. 8.17. These results clearly show that the solution is unstable for $\frac{\Delta r}{\Delta t}$ equal to 1. It was found, in fact, that satisfactory results are obtained when $\frac{\Delta r}{\Delta t}$ is equal to 4, 4 times the greatest velocity in the system. This instability for a small grid ratio is due physically to the fact that local disturbances in the flow propagate at a velocity which is the sum (or difference for left-running waves) of the particle velocity and the local sonic velocity. The solution cannot therefore be proceeded with at a rate faster than the speed of local disturbances (i.e. Δ t cannot be too large for a given Δ r). This criterion accounts for the small discrepancies between the characteristic solution and the finite difference solution for the perfect gas with γ = 1.4 near the escape front, a trend noted in the previous section, (Section 8.4, Fig. 8.12). Since a grid ratio $\frac{\Delta r}{\Delta t}$ of 5 (the escape front velocity) was used in this solution, a slight instability occurs near the escape front where the propagation velocity of local disturbances is comparable to the grid ratio used.

8.6. Similarity Solution for Cylindrical Expansion of Perfect Gas with γ = 1.4

The similarity analysis of Section 5 was

followed to obtain a solution of the expansion for the cylindrical case for times greater than 1 in order to determine at what time the similarity solution becomes a sufficiently accurate discription of the expansion process. Values for the constants B and D (Eqs. 5.20 and 5.21) used for the cylindrical expansion (ν = 1.0) of the perfect gas (γ = 1.4) are

B = 5.0

D = 0.240

A comparison of the results obtained by the similarity solution and those obtained by the finite difference method (for perfect gas with γ = 1.4) at times t = 2.0, 3.0 and 4.0 are shown in Figs. 8.18 to 8.20. The values obtained for the speed of sound at the center by the similarity assumption and the finite difference method respectively are:

t = 2.0	a = 0.568	by similarity
	a = 0.627	by finite difference
t = 3.0	a = 0.484	by similarity
	a = 0.512	by finite difference
t = 4.0	a = 0.432	by similarity
	a = 0.447	by finite difference

The appearance of these curves, and the gradual coalescence of the two solutions into one, indicate that for times

greater than 4 (greater than 4 times the time required for the initial expansion wave to reach the center), the similarity assumptions of Section 5 become sufficiently valid to enable one to obtain an accurate solution by this simple method.

8.7. Shocked States of Real Gas (Aluminum) and the Isentropes Appropriate to Two Shock Strengths

The equation of state constants (Eq. 6.3 and 6.4) appropriate to the shocked states of aluminum are:

$a = 0.5$

$b = 1.63$

$\bar{E}_o = 0.05 \times 10^{12}$ dyne cm/gm

$\bar{A} = 0.752 \times 10^{12}$ dynes/cm^2

$\bar{B} = 0.65 \times 10^{12}$ dynes/cm^2

$\alpha = 5.0$

$\beta = 5.0$

Neglecting $\bar{p}_o$ with respect to $\bar{p}_s$, the shocked metal pressure (in Eq. 6.6), Eqs. 6.3 and 6.6 are simulatneously solved for a series of shock strengths, (values of σ), and the resulting shock Hugoniot for aluminum is shown in Fig. 8.21. Two isentropes are calculated and shown in Fig. 8.21 as well. In the first case, corresponding to an initial shock strength σ of 2.0, the perfect gas equation

(Eq. 6.5) becomes valid at the density $\bar{\rho}$ = 0.52953 gms/cm^3 and a pressure $\bar{p}$ = 0.009771 Mb. The curve fits for "p" and "a" as functions of "ρ" have been obtained and are valid in the range

$$0.52953 \leq \bar{\rho} \leq 5.4$$

The coefficients of the power series are given in Table 1.

The second isentrope calculated is that corresponding to an initial shock strength σ of 1.7, and is also shown in Fig. 8.21. In this case, the internal energy of the gas $\bar{E}$ drops below the critical energy $\bar{E}_g$ at which condensation begins. This occurs at $\bar{\rho}$ = 2.594 gms/cm^3, and the condensed form of the equation of state (Eq. 6.3) becomes valid at this value of density. The calculation of the isentrope is continued until $\bar{p}$ = 0, a condition which occurs at $\bar{\rho}$ = 2.320 gms/cm^3. The isentrope is then curve fitted over the range

$$2.320 \leq \bar{\rho} \leq 4.59$$

The coefficients for the polynomials obtained for "p" and "a" as functions of "ρ" are given in Table 2. The critical density at which the pressure becomes negative (i.e. material is in tension) is defined to be the yield point of the metal and the pressure and speed of sound at this point are defined to be zero.

8.8 Solution for Cylindrical Expansion of Real Gas with Shock Strength $\sigma = 2.0$

The finite difference approach using the variables ρ and u (Section 6) has been used to obtain a solution of the expansion of the shocked aluminum ($\sigma = 2.0$) using the two curve fits $[p = f(\rho) ; a = g(\rho)]$ of Section 8.7 to describe the metal states. The distributions of ρ and u at times t = 0.5, 1.0, 2.0 and 3.0 for a cylindrical expansion are shown in Figs. 8.22 and 8.23, and are of essentially the same character as the corresponding distributions for the perfect gas ($\gamma = 3.0$) expansion.

A comparison of the real gas ($\sigma = 2.0$) and the perfect gas ($\gamma = 3.0$) solutions for the density distributions as functions of r at times t = 0.5, 1.0 and 2.0 are shown in Figs. 8.24 to 8.26. A slight discrepancy is immediately noted as to the location of the point of zero density, the escape front. For the perfect gas case, the escape front velocity is 1, for the real gas case, the escape front velocity has been found to be 0.81243. The greatest discrepancy in the two solutions at time t = 0.5 (Fig. 8.24) occurs in the low density, highly-expanded region, where the effective γ calculated from the strong shock approximation is no longer valid.

As time increases, the disagreement between the two solutions becomes increasingly apparent and by time t = 2.0 (Fig. 8.26), the real gas solution yields a value of at the center of 0.200, whereas the perfect gas approximation yields a value of .230.

The perfect gas approximation is thus sufficient to describe the expansion of shocked aluminum for this shock strength for very short times in the high-density region, but becomes increasingly inaccurate as time increases.

8.9 Solution of Cylindrical Expansion of Real Gas With Shock Strength σ = 1.7

The impact velocity required to produce a shock of given strength in a metal is given approximately by:

$$\bar{V} = \sqrt{3\,\bar{E}_s} \qquad 8.2$$

where $\bar{E}_s$ is the internal energy of the shocked gas, and $\bar{V}$ is the velocity of impact. It is found that to produce a shock of strength σ = 2.0, an impact velocity of 15.67 km/sec is required. Since such a velocity is not experimentally obtainable, although meteorite impacts do occur in this velocity range, it was decided to obtain a solution for the expansion of a metal which is not so strongly shocked.

The isentrope for a shock strength σ = 1.7 in aluminum has been obtained (Section 8.7), this shock strength corresponding to an impact velocity of 10.06 km/sec. The cylindrical expansion results have been obtained using the finite difference method with variables ρ and u, and using the polynomial curve fits "p"and"a"appropriate to this particular isentrope (Section 8.7).

The density profiles for times t = 0.25, 0.50, 1.00 and 1.25 are shown in Fig. 3.27. It is seen that as time progresses the point at which the critical density is reached moves radially inward, the critical density being the density at which the material fails in tension. At t = .25, the critical radius is 1.053, at t = 0.5, it is 1.047, at t = 1.0 it is 0.3647, and at t = 1.25 it is 0.653. For t = 1.35, the solution indicates that the density is below its critical value for all radii, and the specimen can be considered to have failed in its entirety.

EFFECT OF TIME ON SONIC VELOCITY DISTRIBUTION

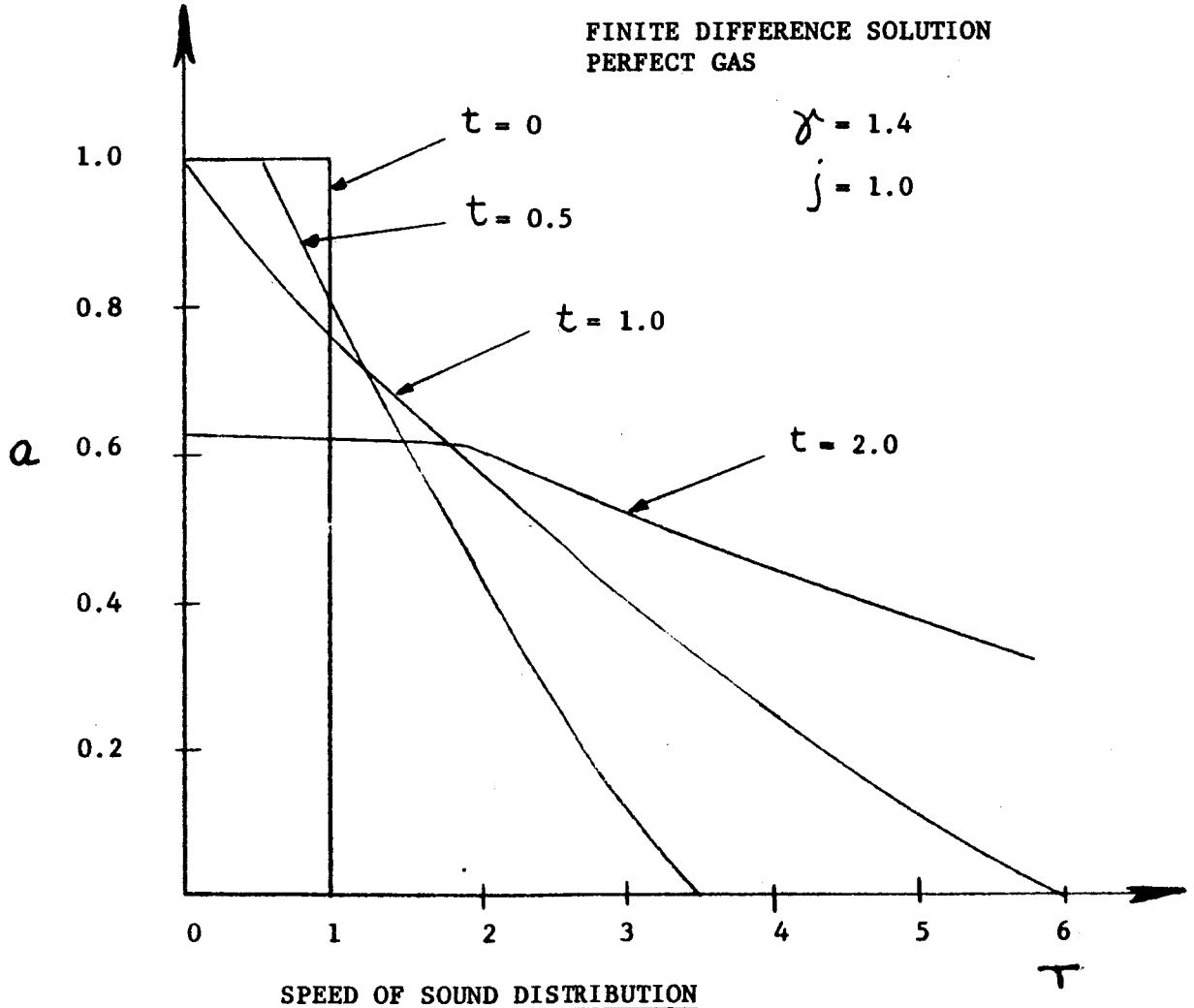

SPEED OF SOUND DISTRIBUTION

FIG. 8.1

EFFECT OF TIME ON DENSITY DISTRIBUTION

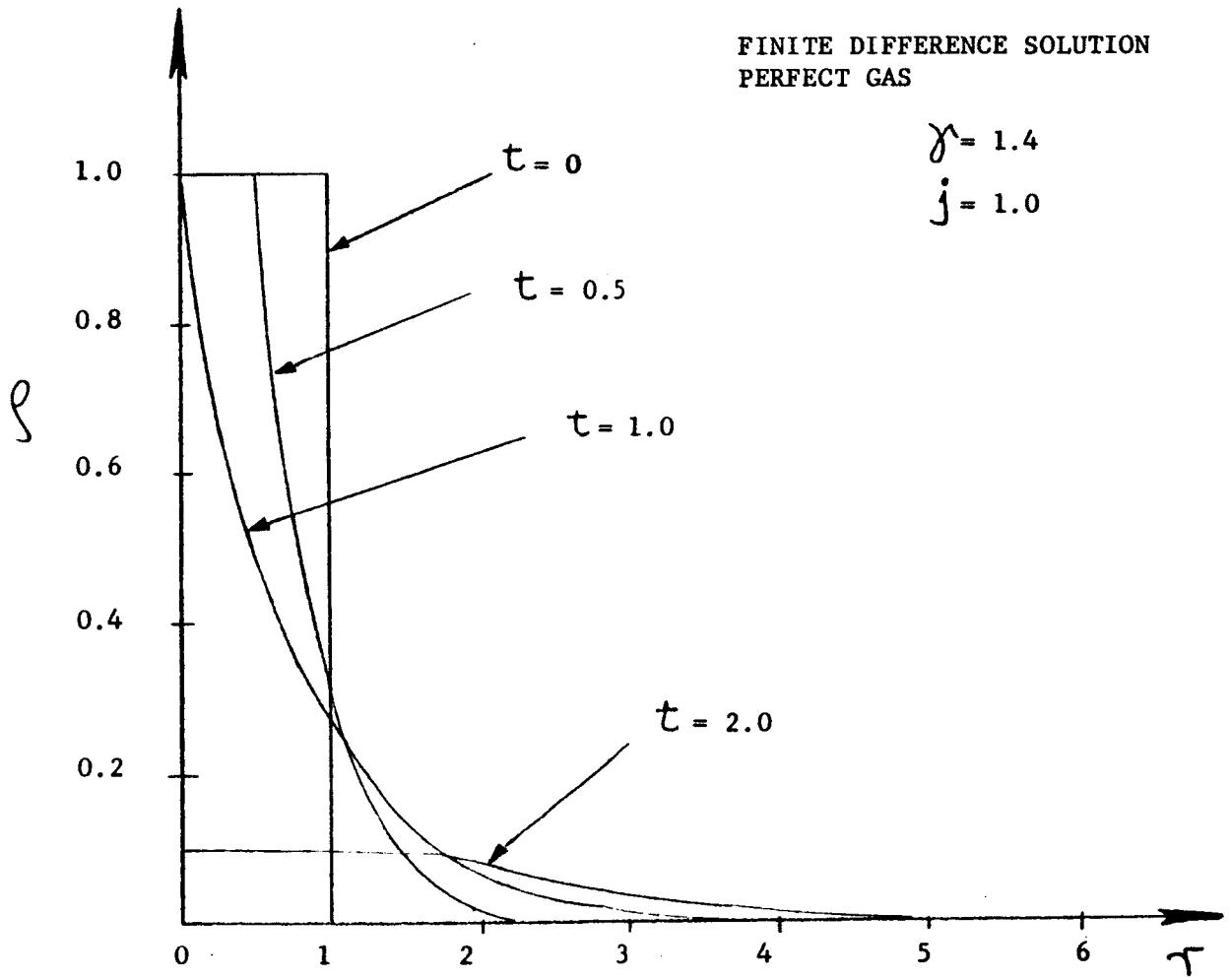

DENSITY DISTRIBUTION

FIG. 8.2

EFFECT OF TIME ON PARTICLE VELOCITY DISTRIBUTION

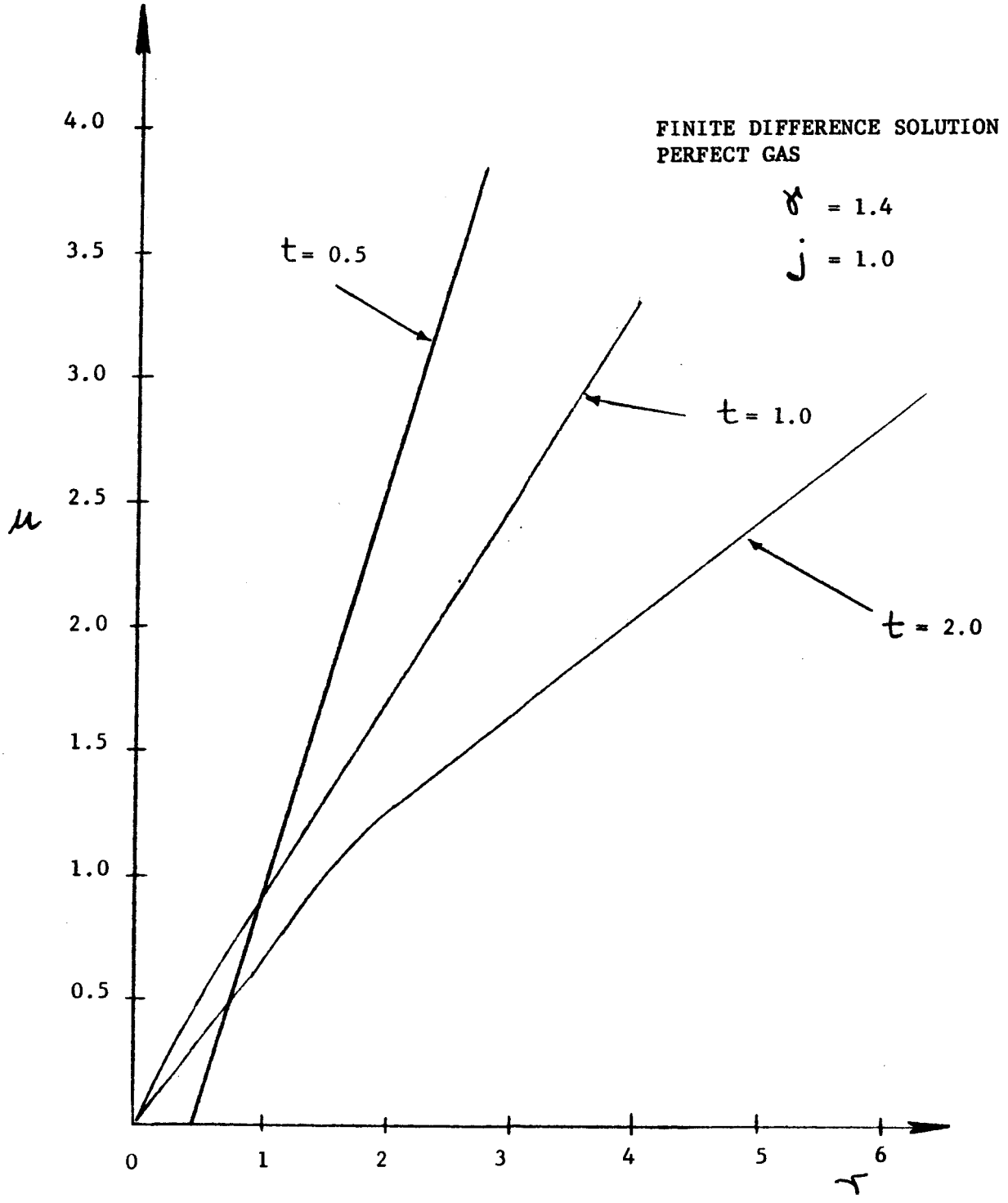

VELOCITY PROFILE

FIG. 8.3

EFFECT OF TIME ON SONIC VELOCITY DISTRIBUTION
IN PLANE GEOMETRY

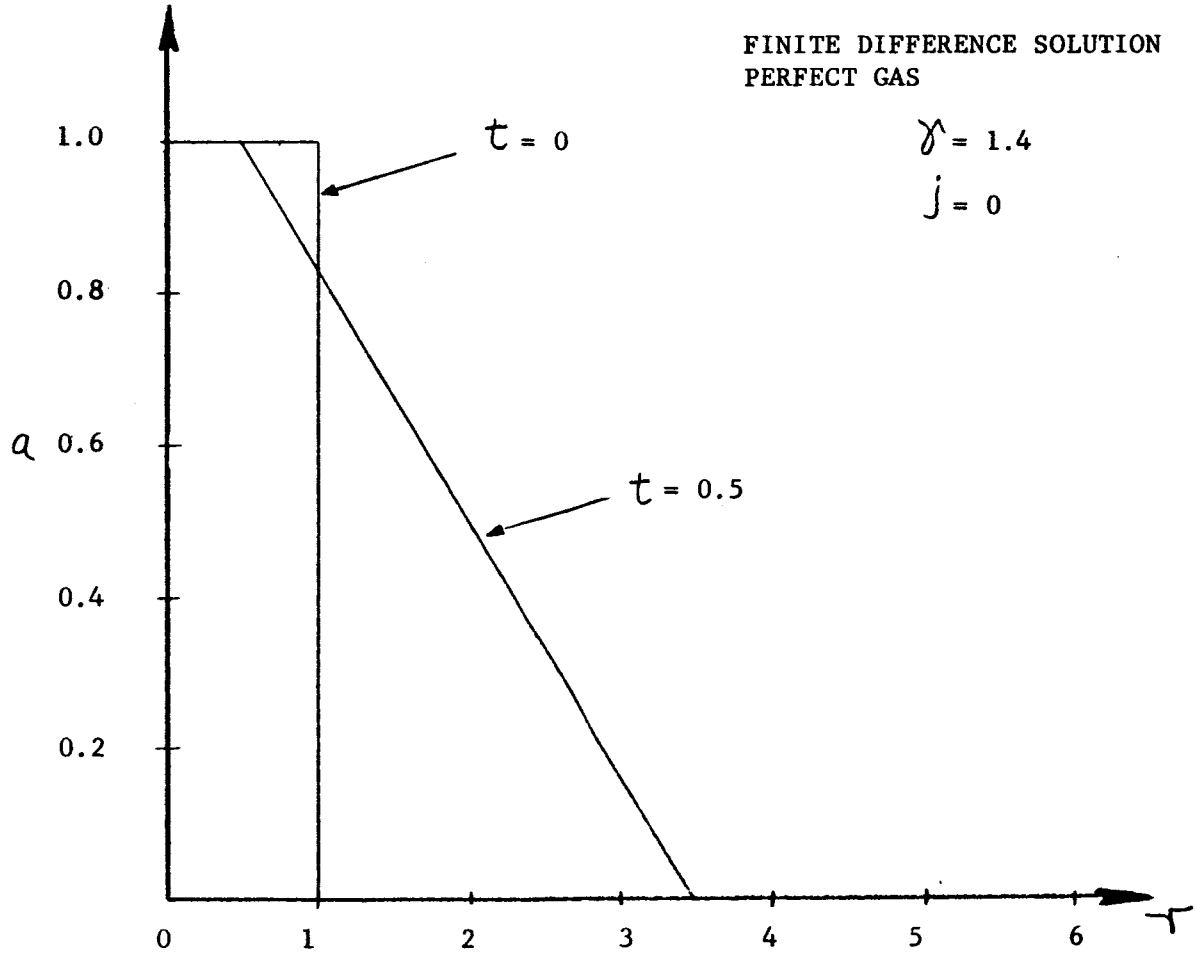

SPEED OF SOUND DISTRIBUTION

FIG. 8.4

EFFECT OF GEOMETRY ON SONIC VELOCITY DISTRIBUTION

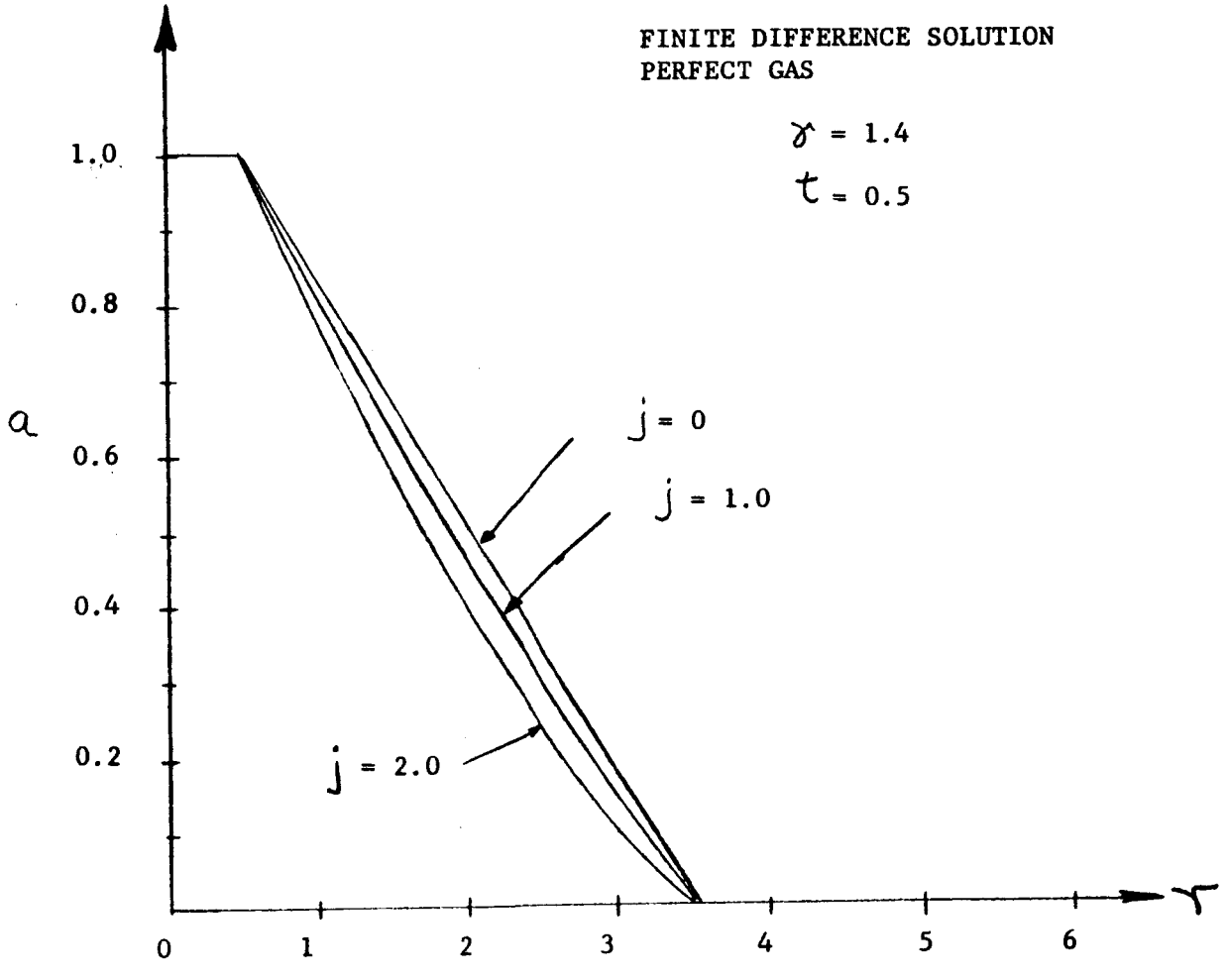

SPEED OF SOUND DISTRIBUTION

FIG. 8.5

EFFECT OF GEOMETRY ON SONIC VELOCITY DISTRIBUTION

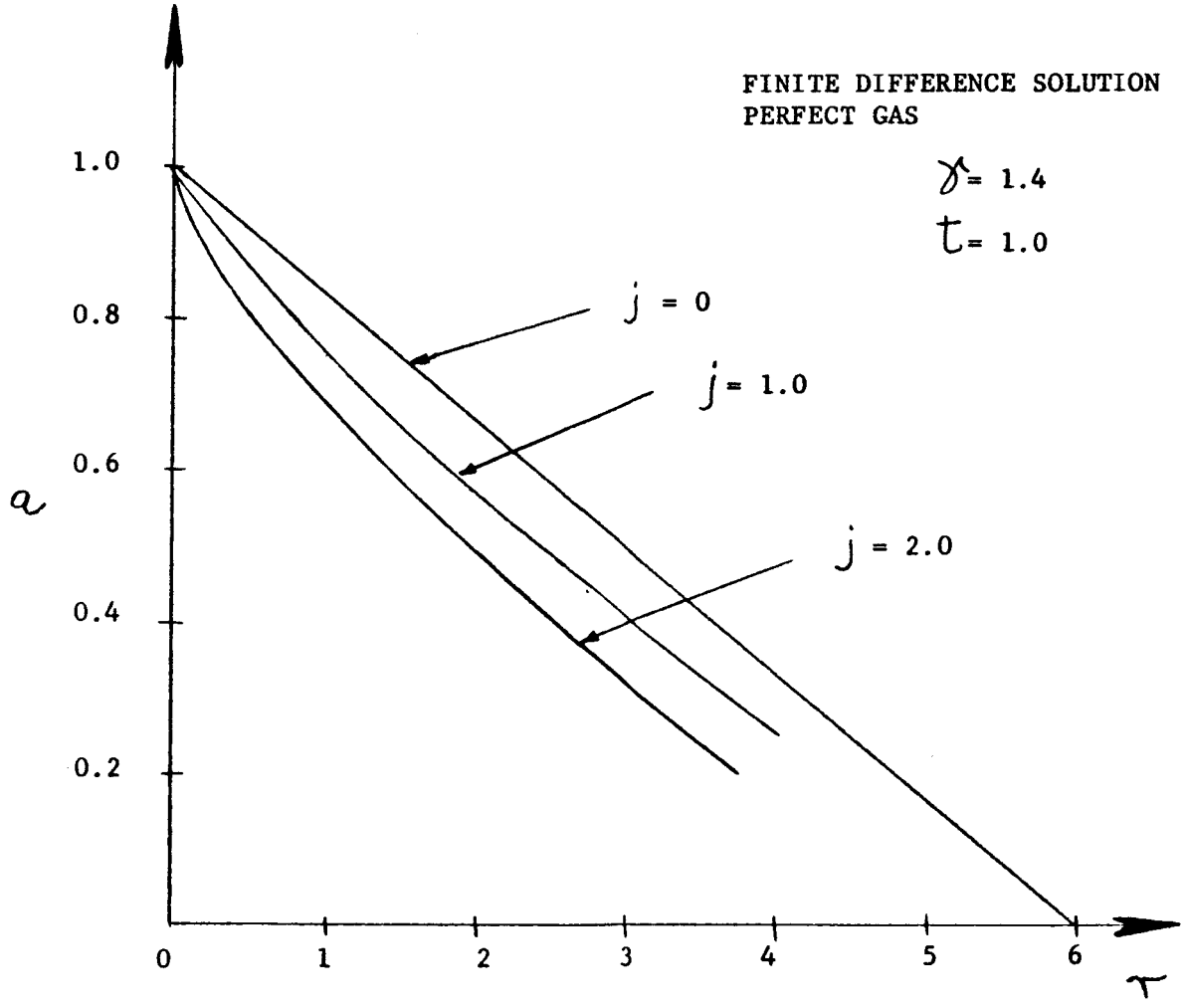

SPEED OF SOUND DISTRIBUTION

FIG. 8.6

EFFECT OF GEOMETRY ON SONIC VELOCITY DISTRIBUTION

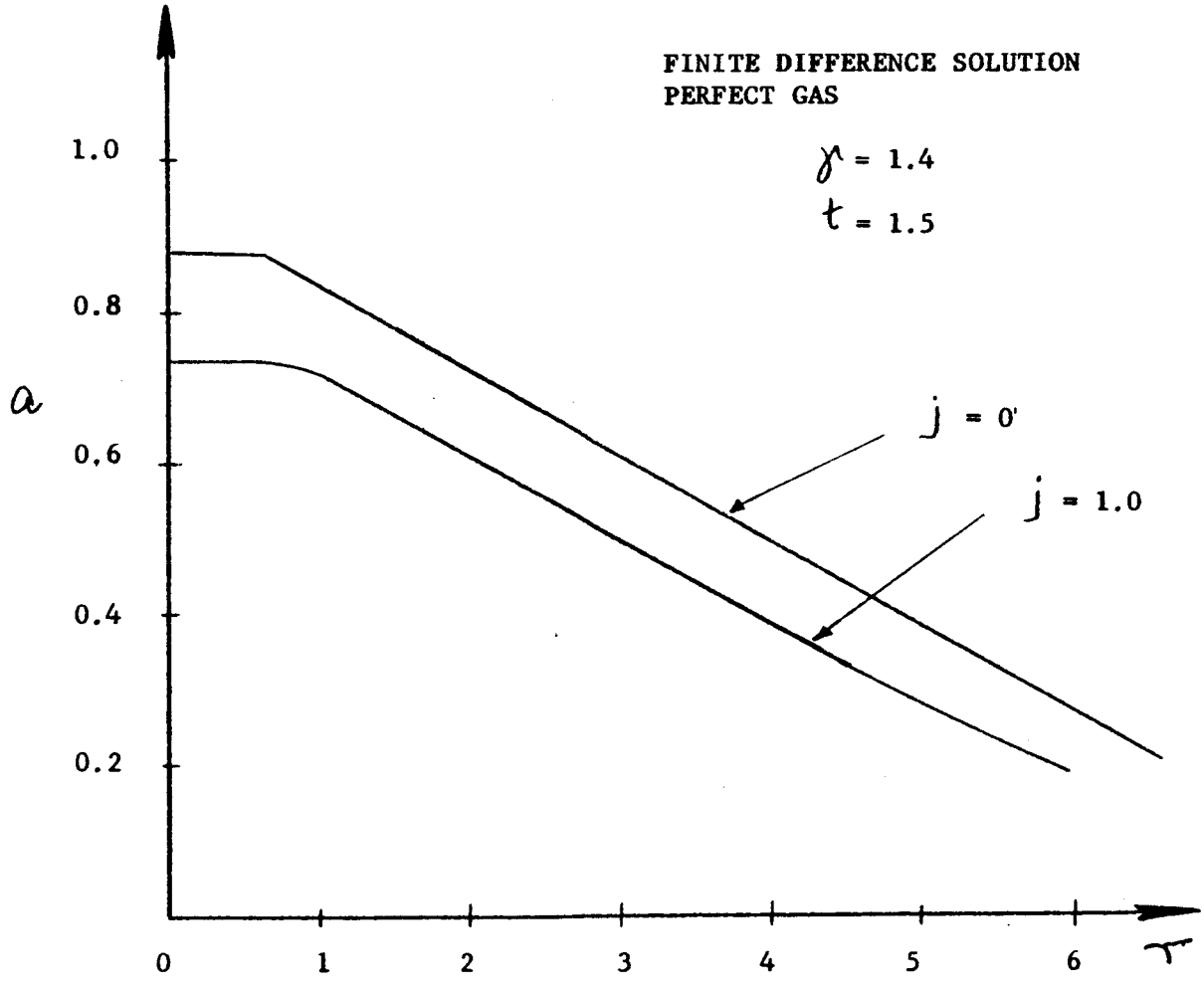

SPEED OF SOUND DISTRIBUTION

FIG. 8.7

EFFECT OF γ ON SONIC VELOCITY DISTRIBUTION

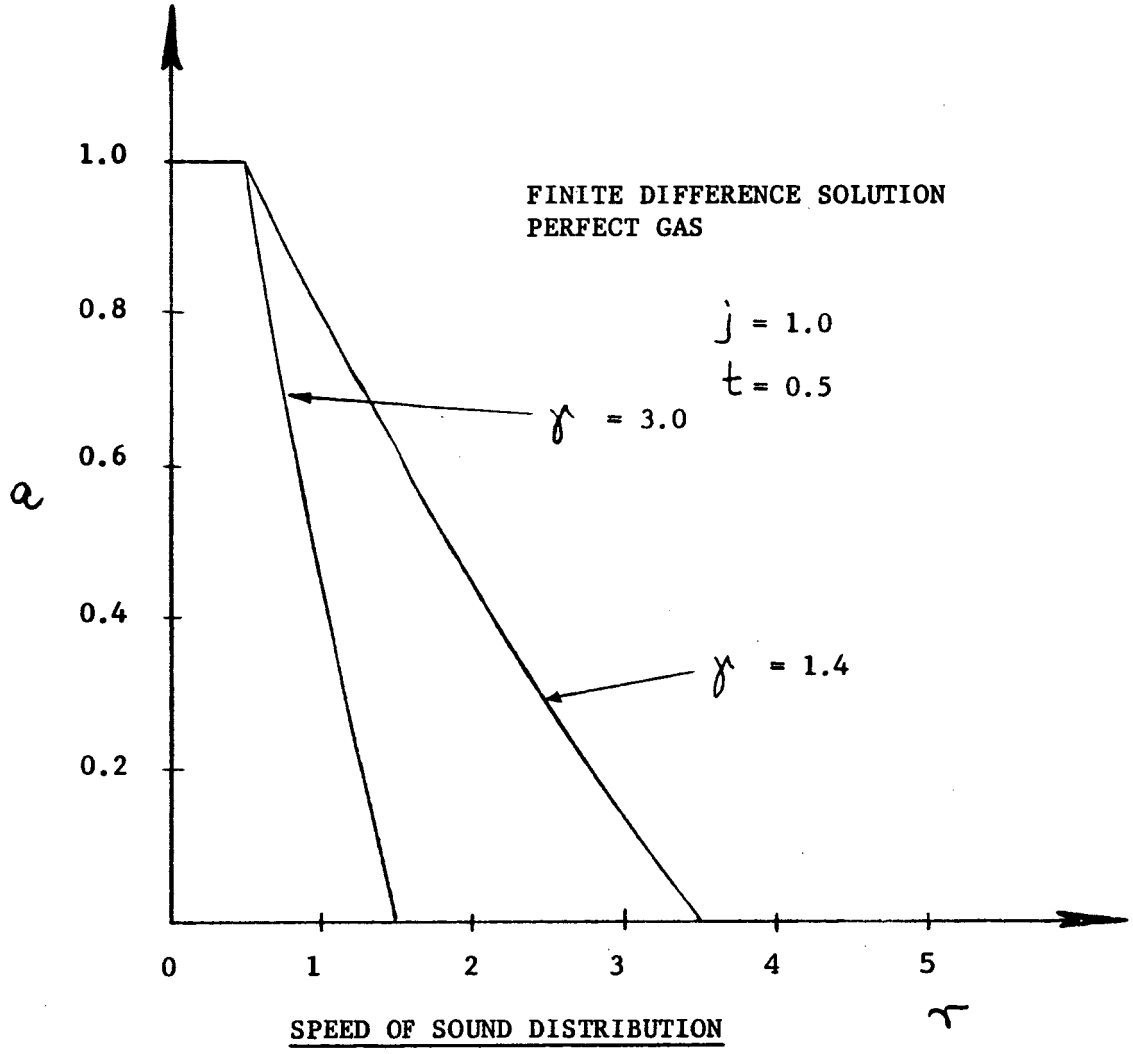

SPEED OF SOUND DISTRIBUTION

FIG. 8.8

EFFECT OF γ ON PARTICLE VELOCITY DISTRIBUTION

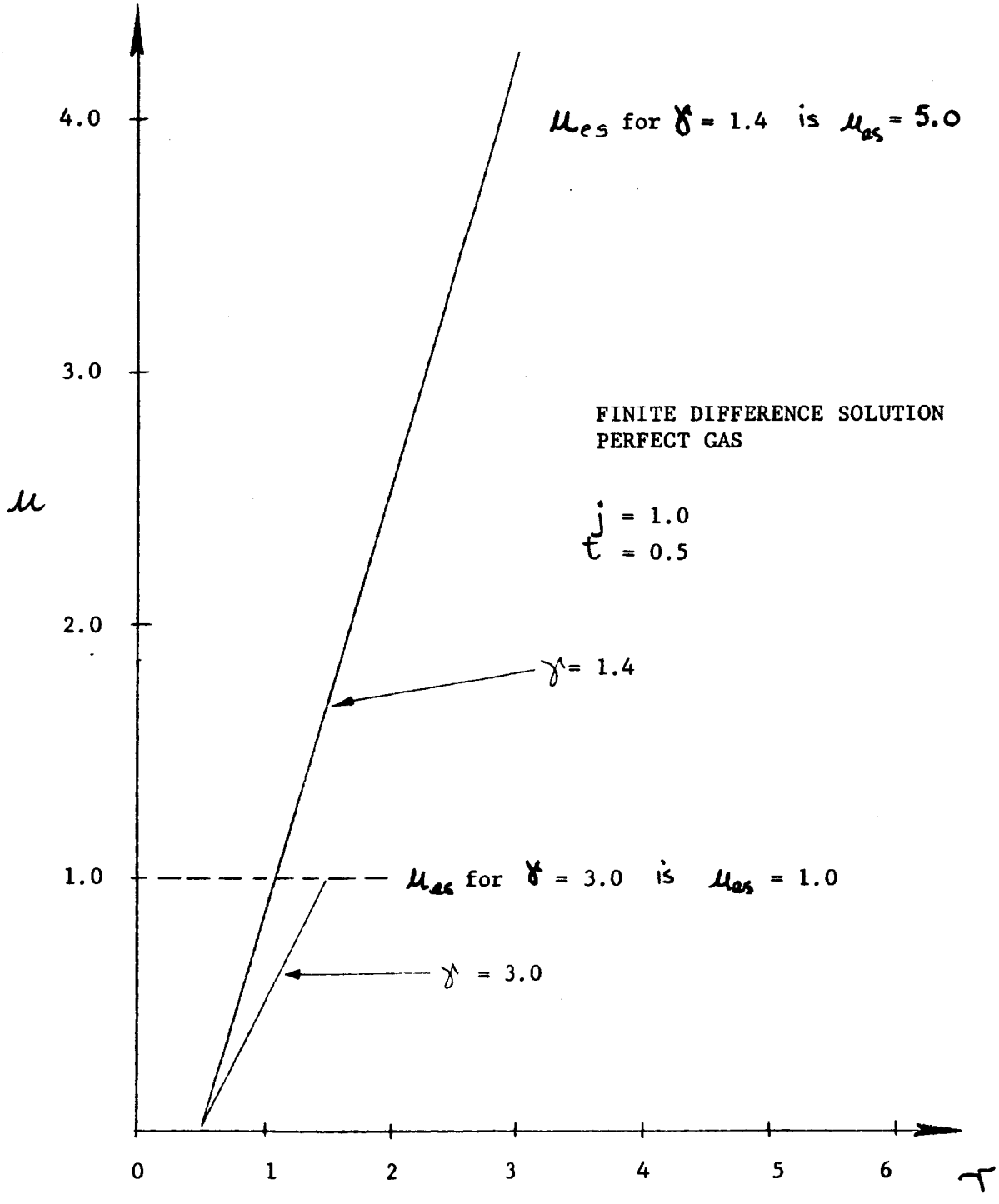

VELOCITY DISTRIBUTION

FIG. 8.9

EFFECT OF γ ON SONIC VELOCITY DISTRIBUTION

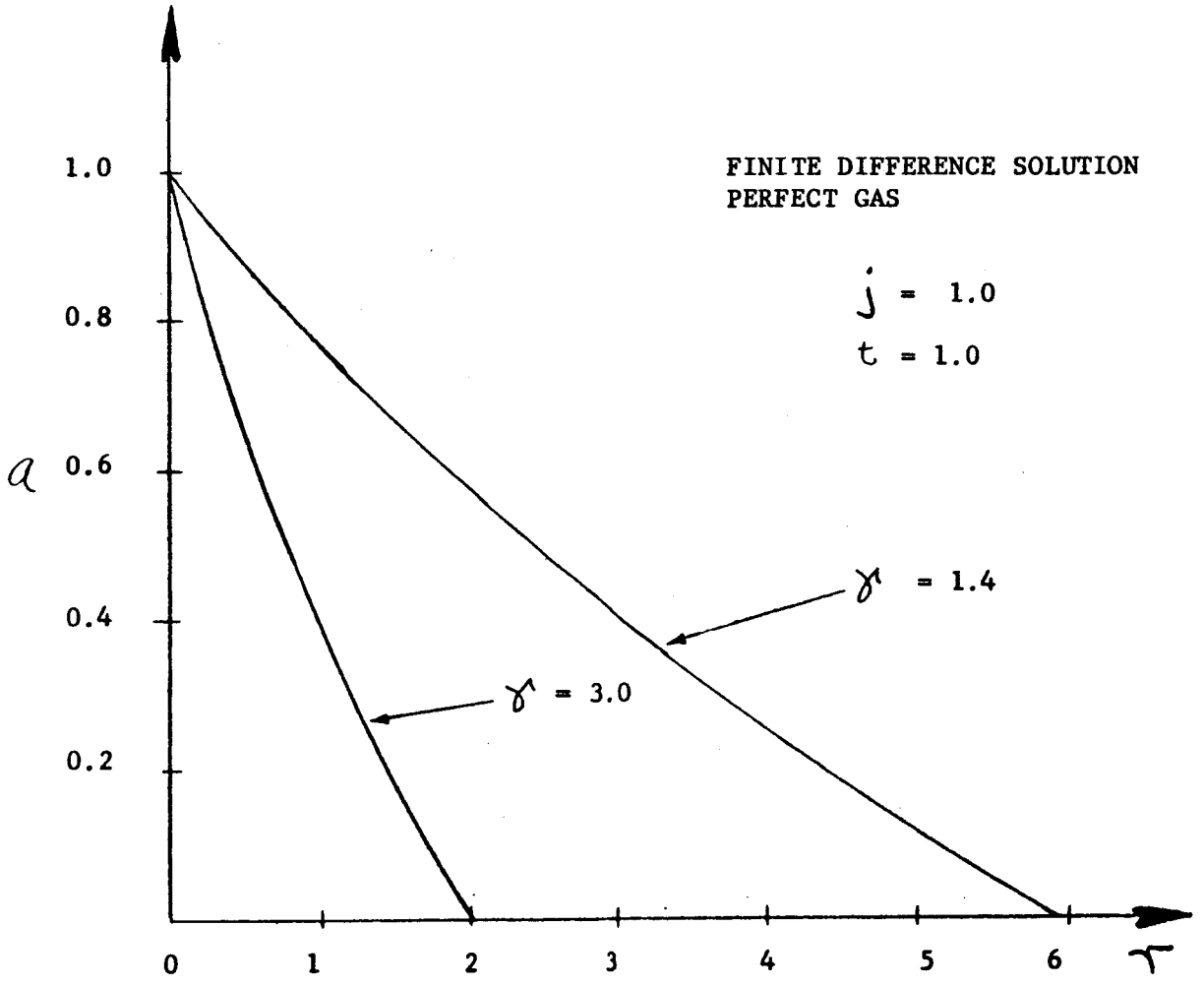

SPEED OF SOUND DISTRIBUTION

FIG. 8.10

EFFECT OF γ ON SONIC VELOCITY DISTRIBUTION

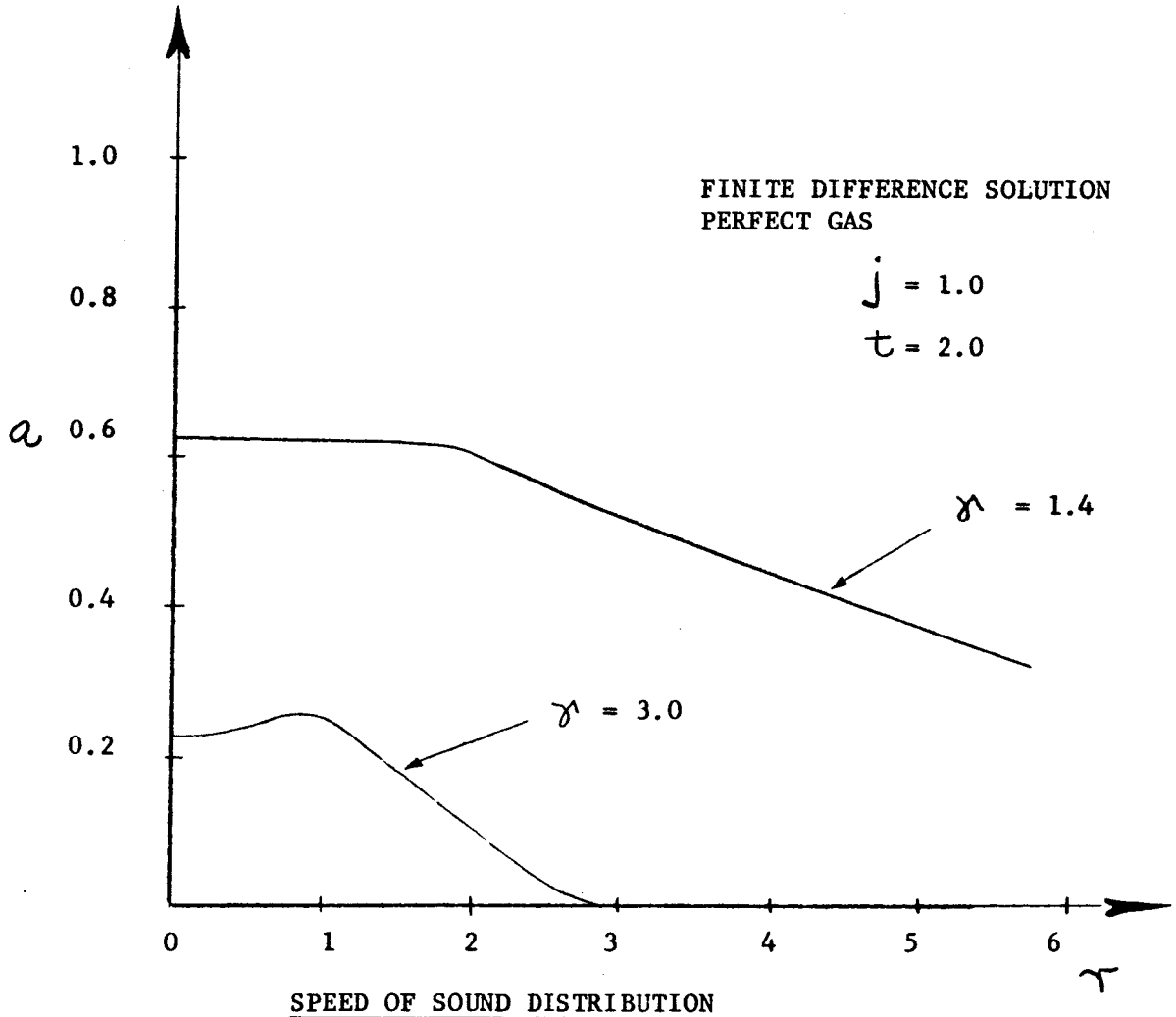

SPEED OF SOUND DISTRIBUTION

FIG. 8.11

COMPARISON OF FINITE DIFFERENCE AND CHARACTERISTIC SOLUTIONS FOR SONIC VELOCITY DISTRIBUTION

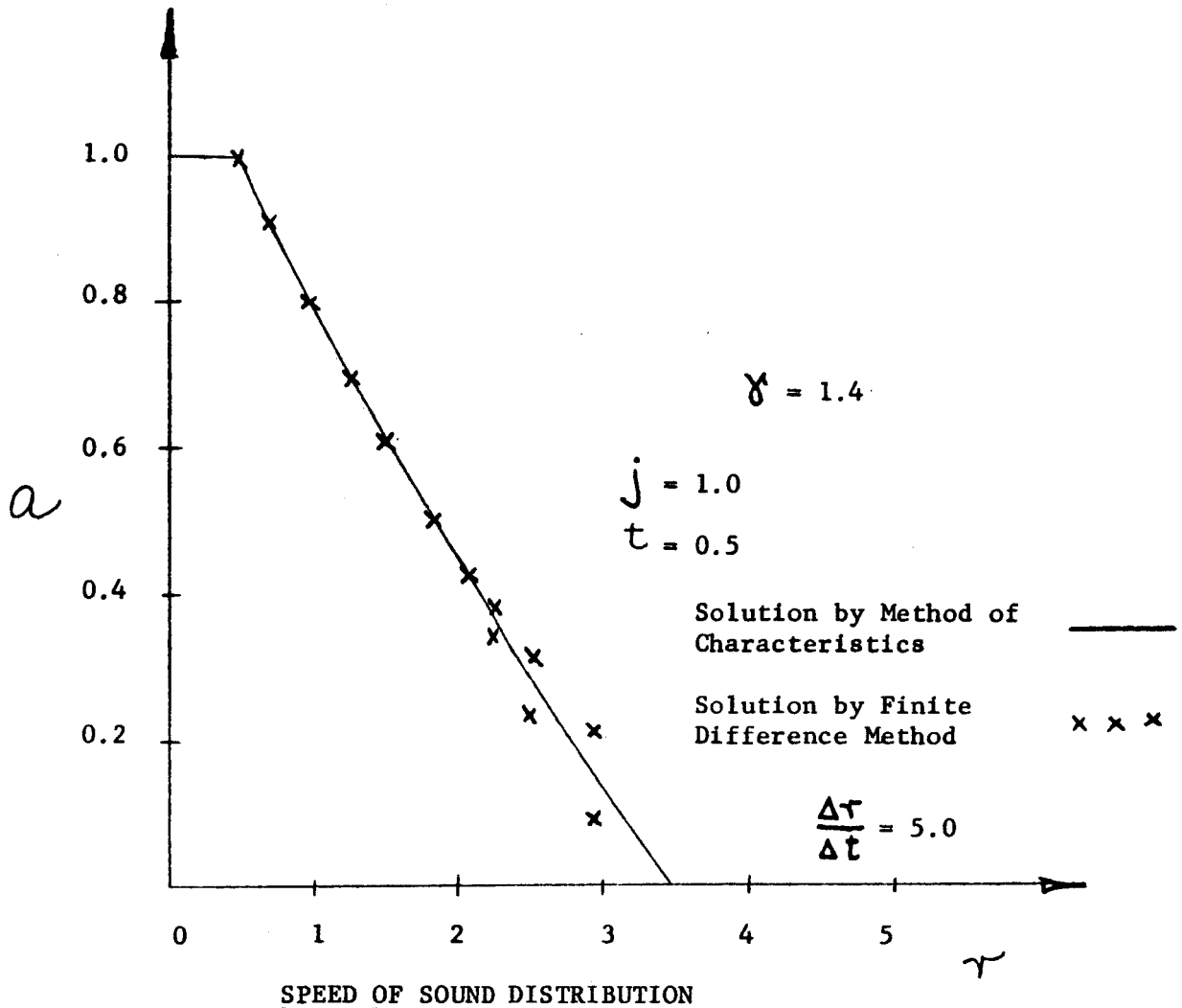

SPEED OF SOUND DISTRIBUTION

FIG. 8.12

COMPARISON OF FINITE DIFFERENCE AND CHARACTERISTIC

SOLUTIONS FOR SONIC VELOCITY DISTRIBUTION

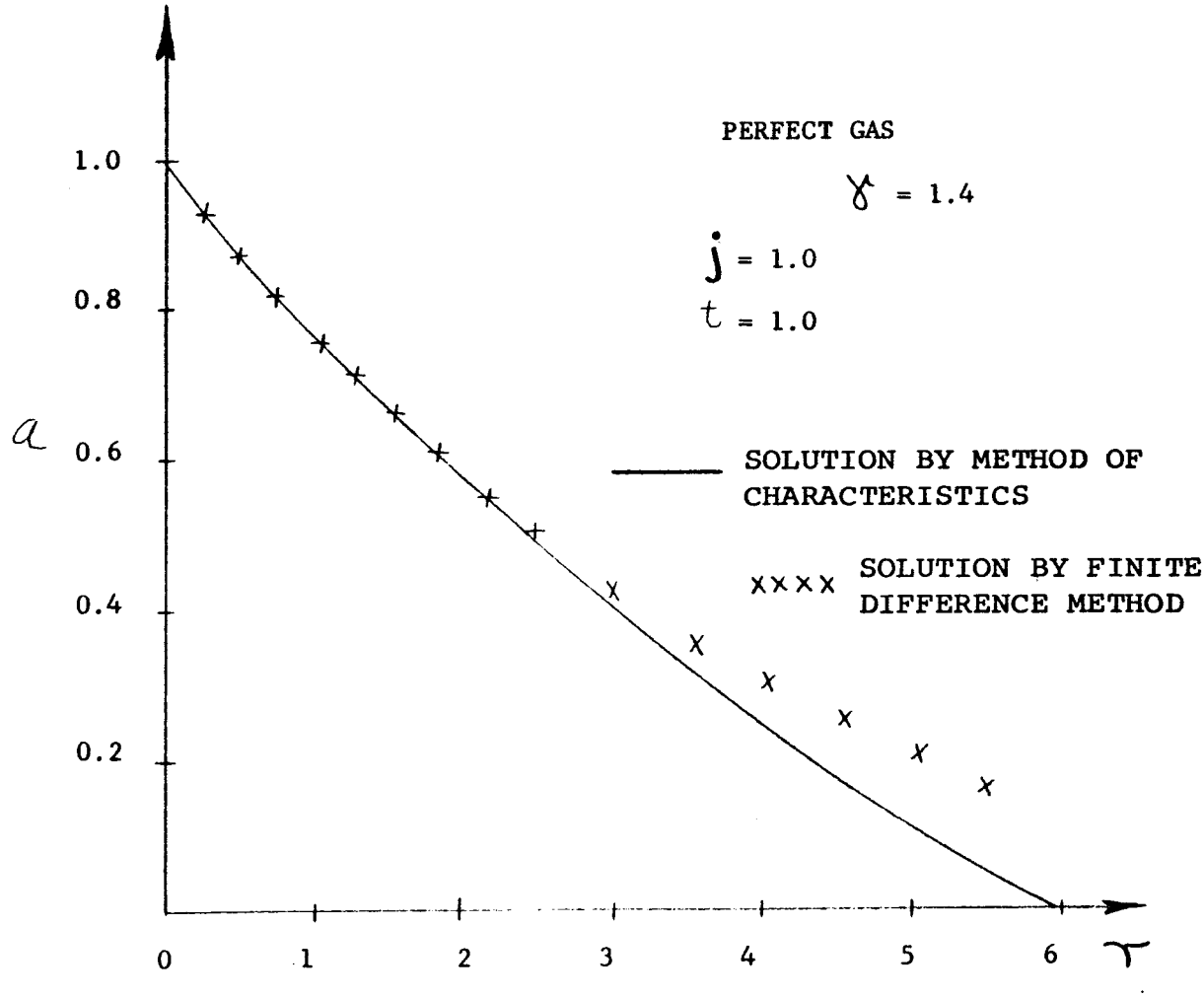

SPEED OF SOUND DISTRIBUTION

FIG. 8.13

COMPARISON OF FINITE DIFFERENCE AND CHARACTERISTIC

SOLUTIONS FOR SONIC VELOCITY DISTRIBUTION

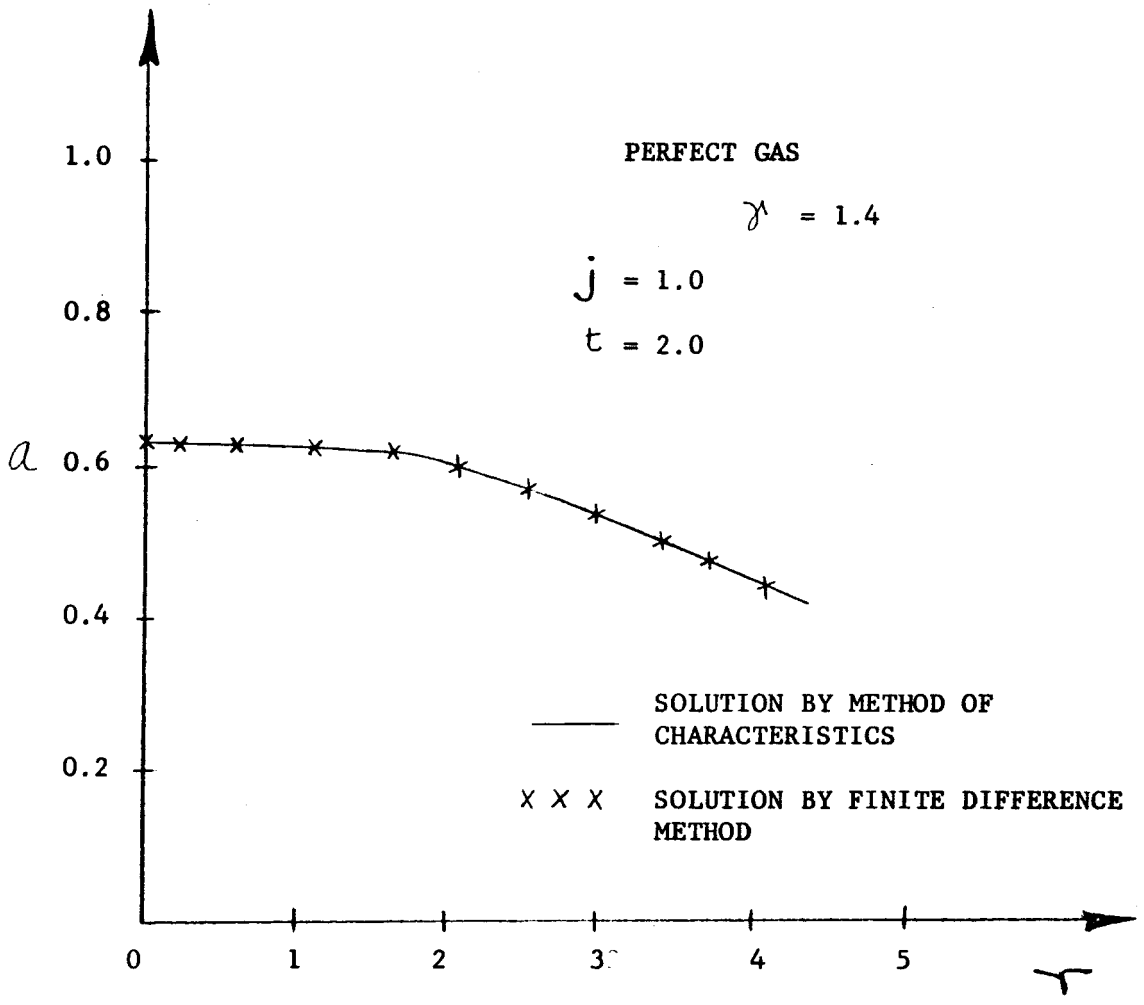

SPEED OF SOUND DISTRIBUTION

FIG. 8.14

COMPARISON OF FINITE DIFFERENCE AND CHARACTERISTIC

SOLUTIONS FOR SONIC VELOCITY DISTRIBUTION

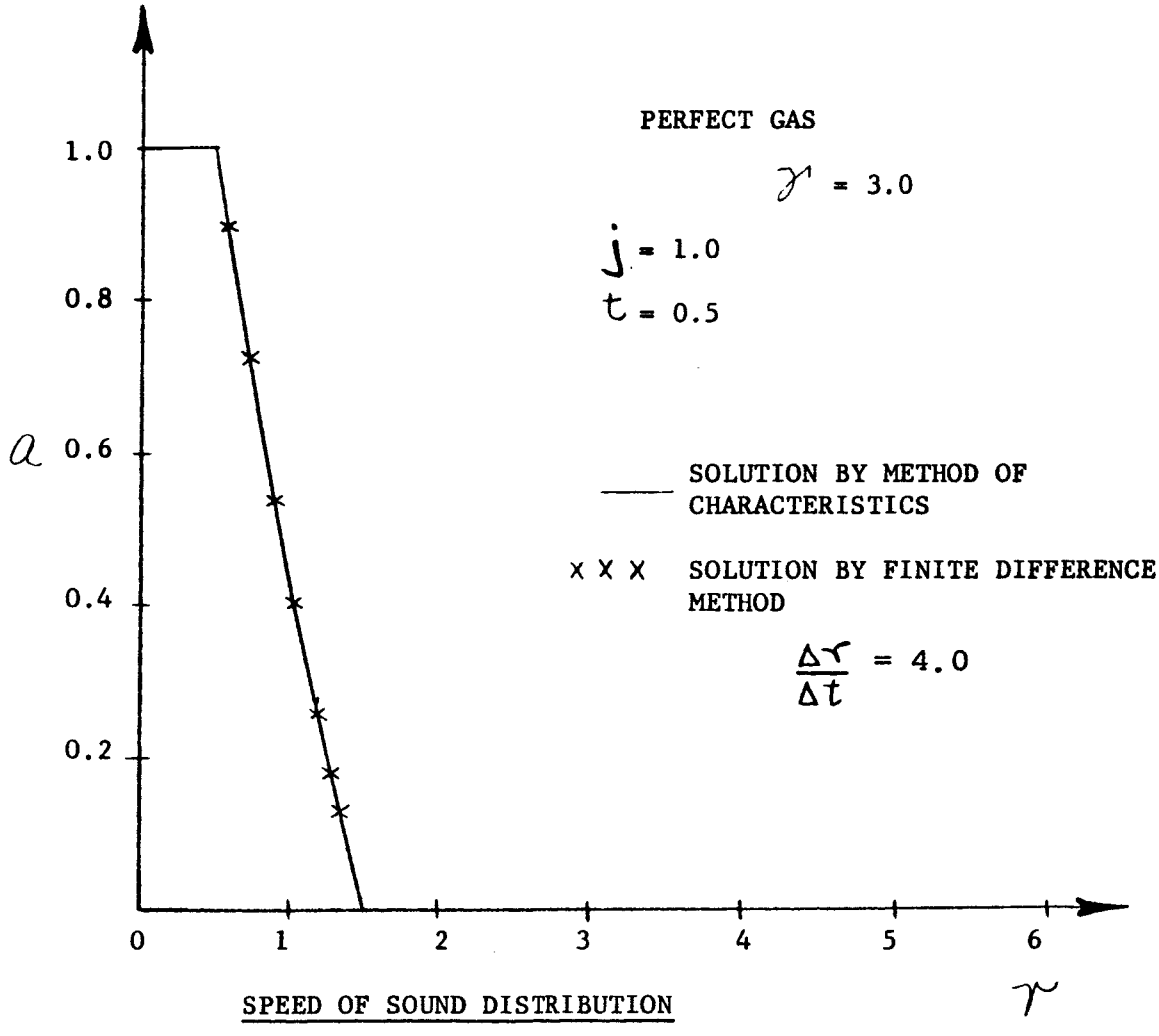

SPEED OF SOUND DISTRIBUTION

FIG. 8.15

COMPARISON OF FINITE DIFFERENCE AND CHARACTERISTIC

SOLUTIONS FOR SONIC VELOCITY DISTRIBUTION

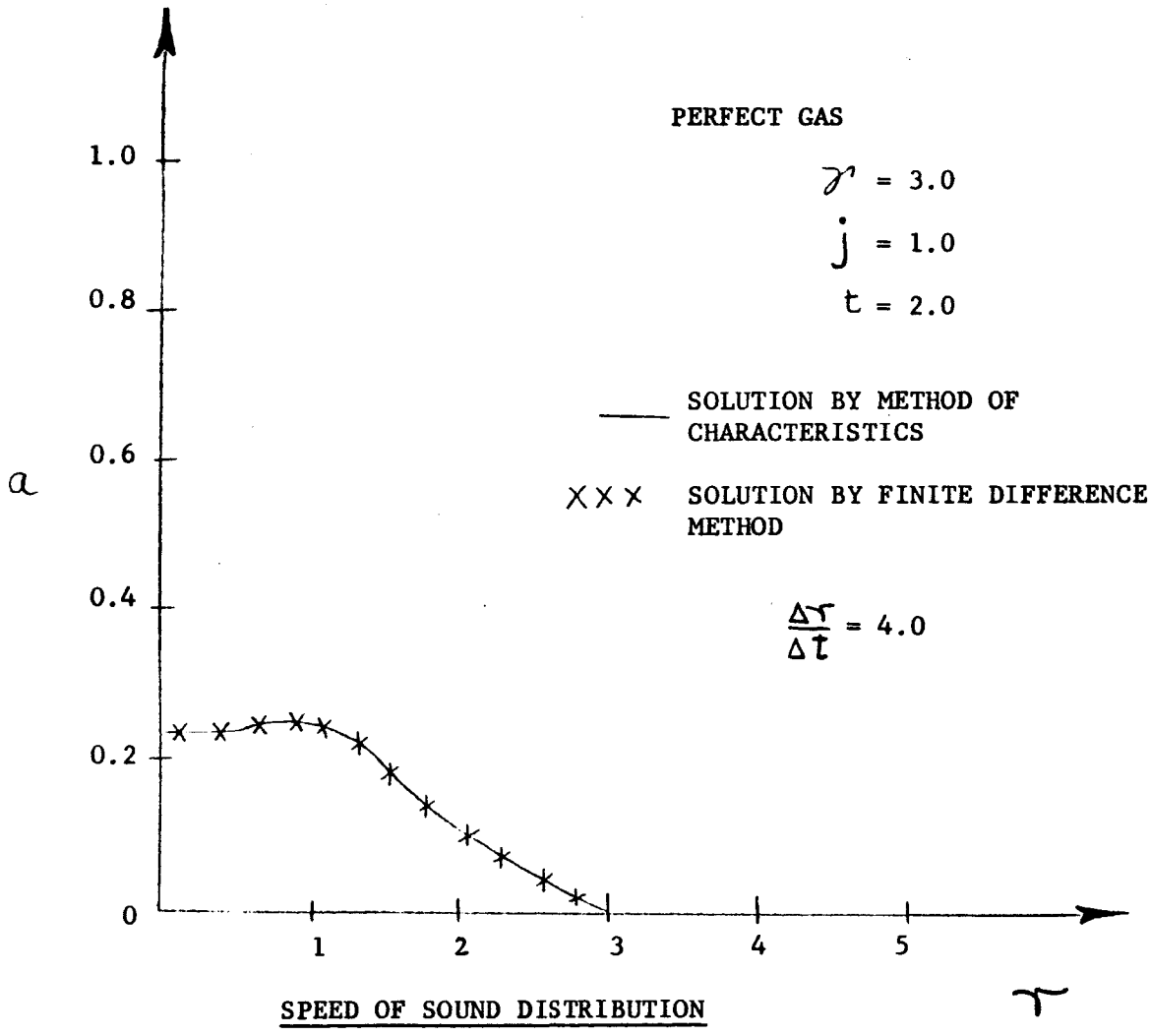

SPEED OF SOUND DISTRIBUTION

FIG. 8.16

EFFECT OF GRID RATIO ON FINITE DIFFERENCE

SOLUTION FOR SONIC VELOCITY DISTRIBUTION

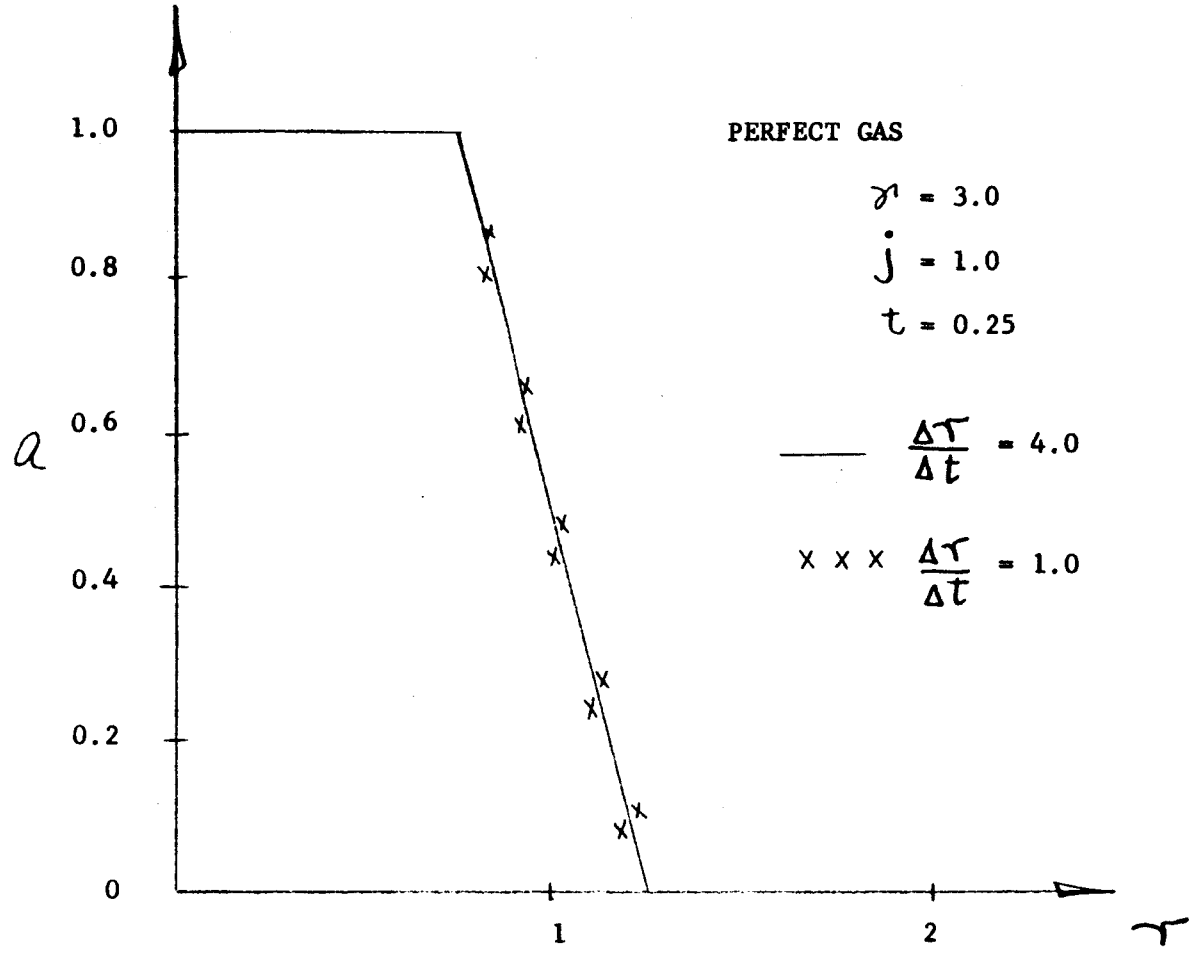

SPEED OF SOUND DISTRIBUTION

FIG. 8.17

COMPARISON OF FINITE DIFFERENCE AND SIMILARITY SOLUTIONS FOR SONIC VELOCITY DISTRIBUTIONS AT TIME $t = 2.0$

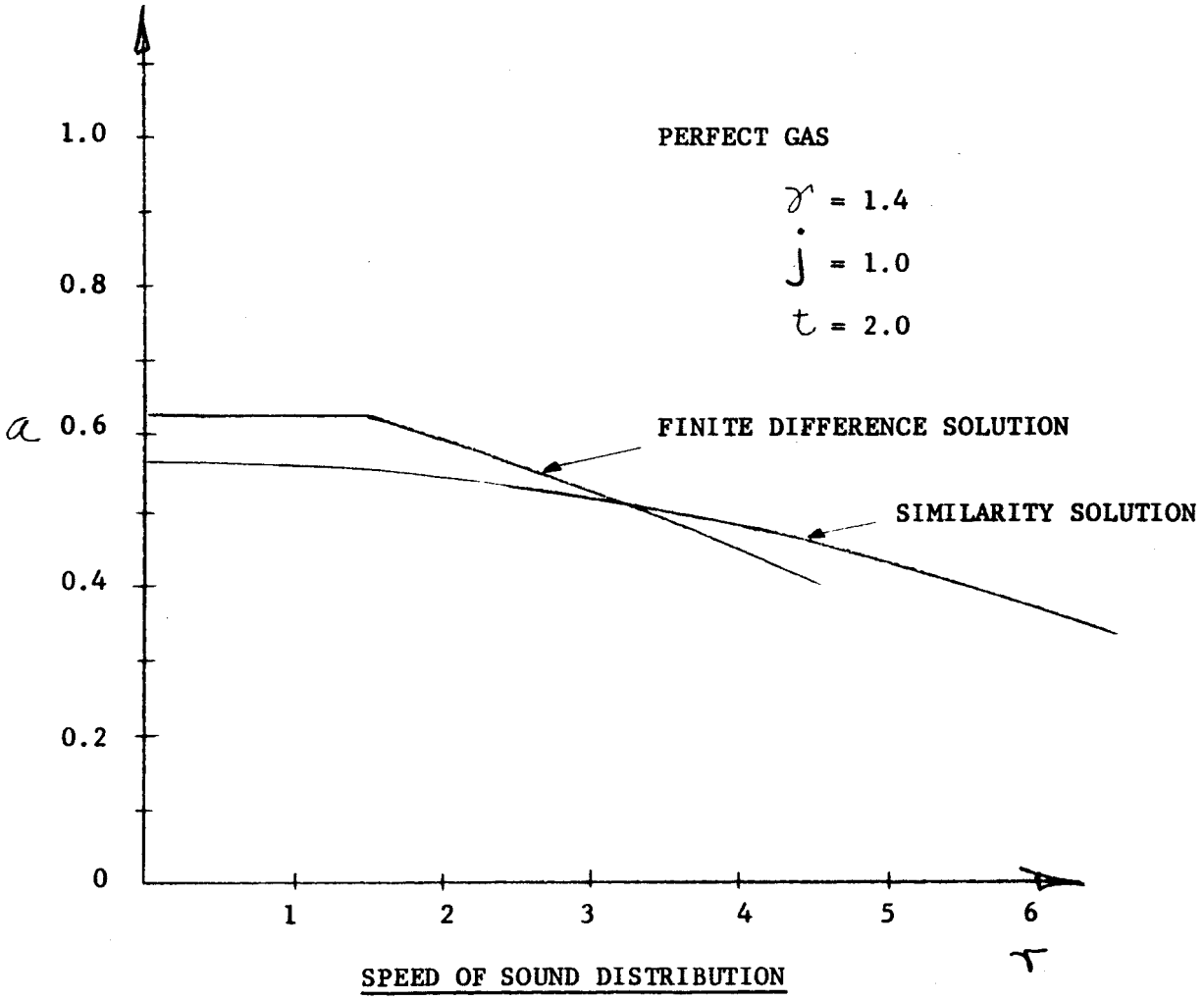

SPEED OF SOUND DISTRIBUTION

FIG. 8.18

COMPARISON OF FINITE DIFFERENCE AND SIMILARITY SOLUTIONS FOR SONIC VELOCITY DISTRIBUTIONS AT TIME $t = 3.0$

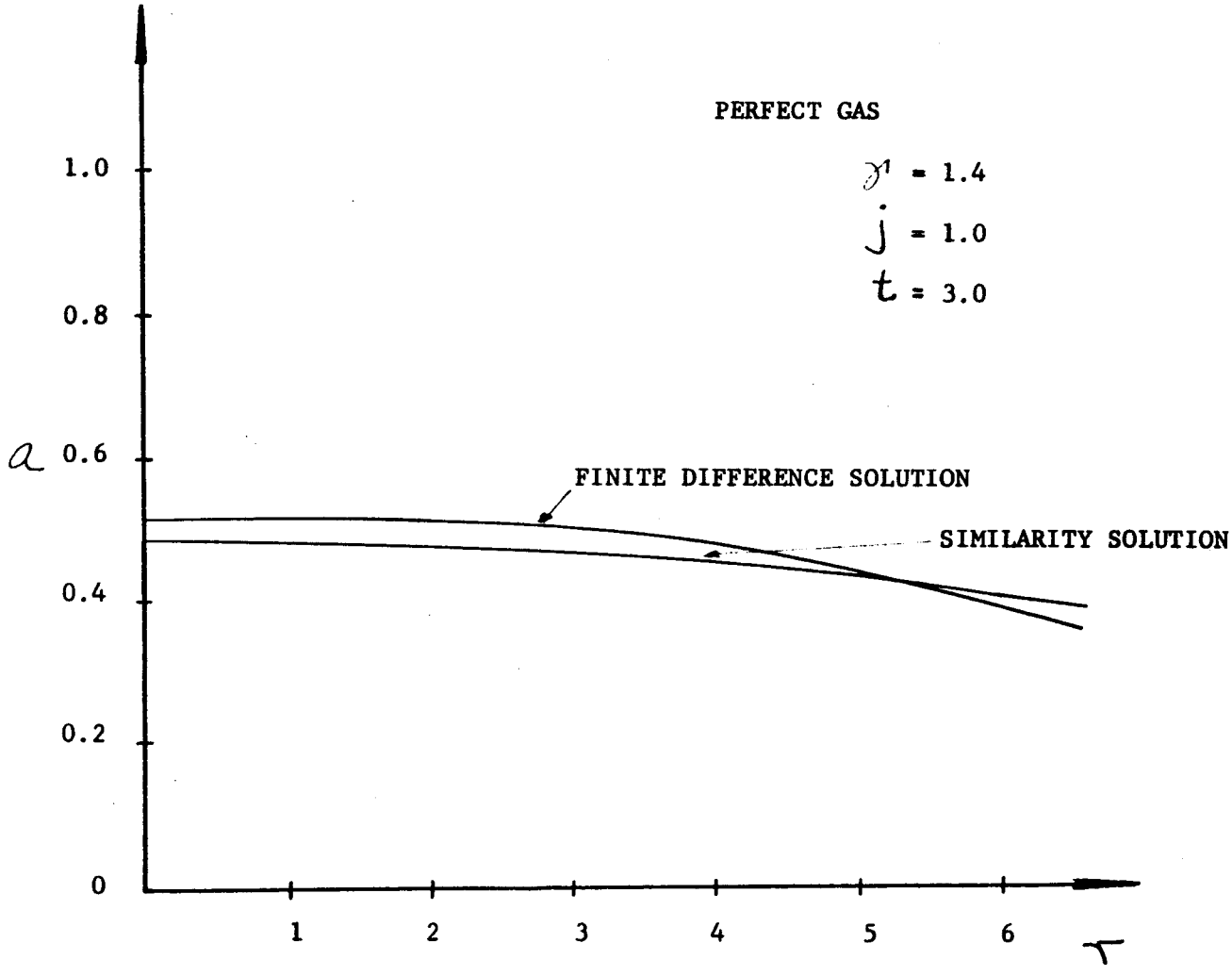

SPEED OF SOUND DISTRIBUTION

FIG. 8.19

COMPARISON OF FINITE DIFFERENCE AND SIMILARITY SOLUTIONS FOR SONIC VELOCITY DISTRIBUTIONS AT TIME $t = 4.0$

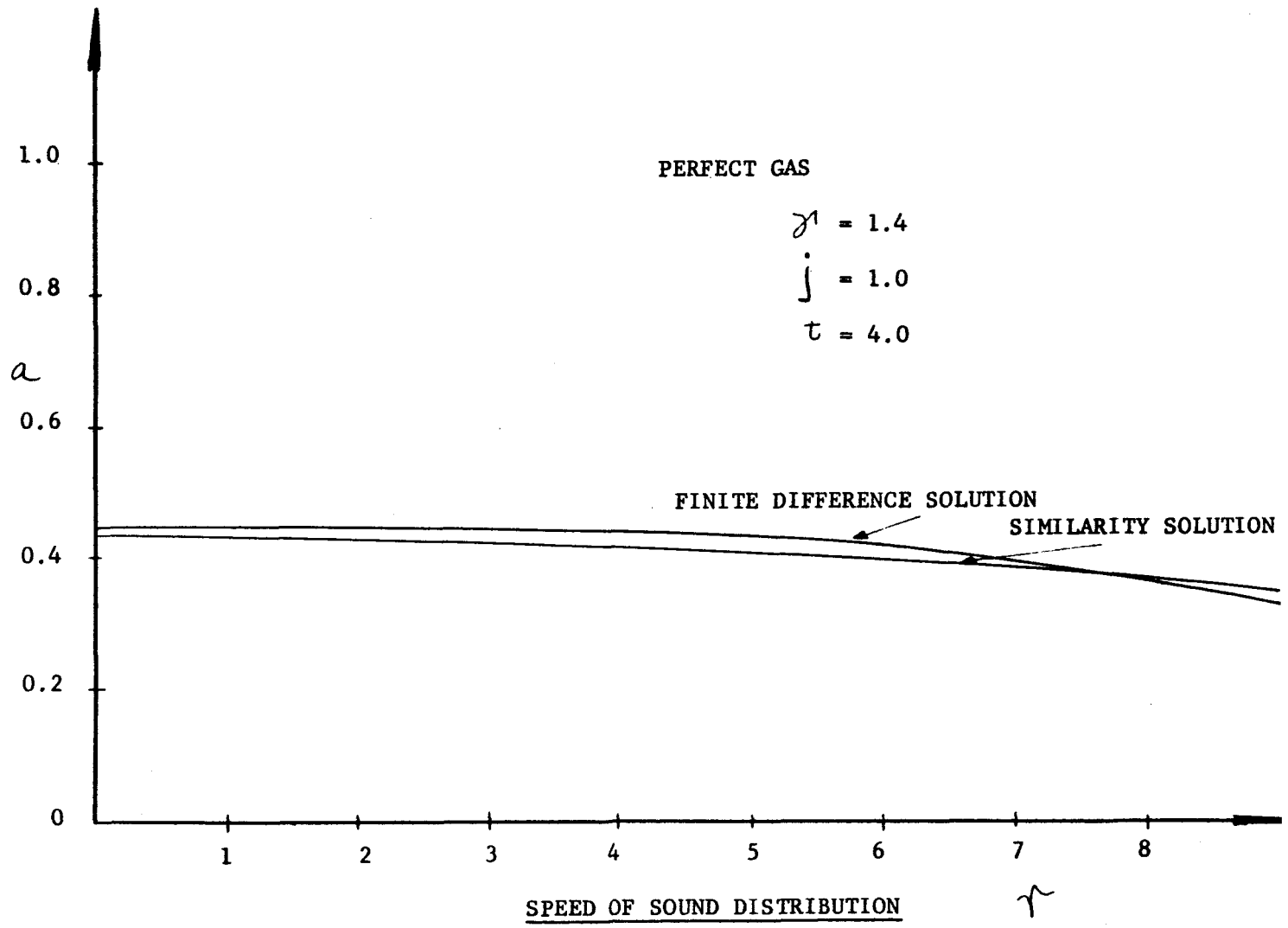

SPEED OF SOUND DISTRIBUTION

FIG. 8.20

FIG. 8.21

SHOCK HUGONIOT AND TWO ISENTROPES OF ALUMINUM

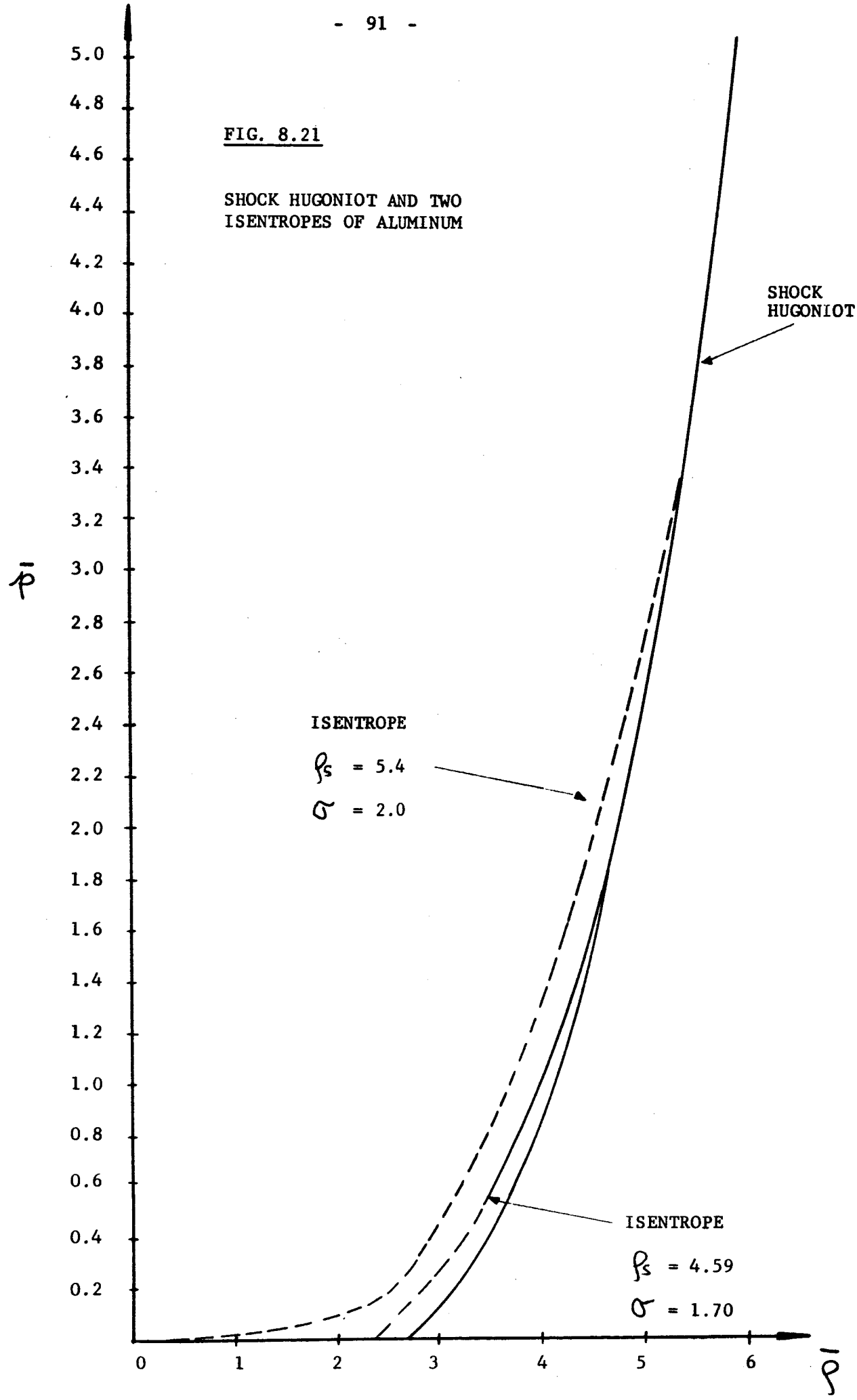

EFFECT OF TIME ON DENSITY DISTRIBUTION

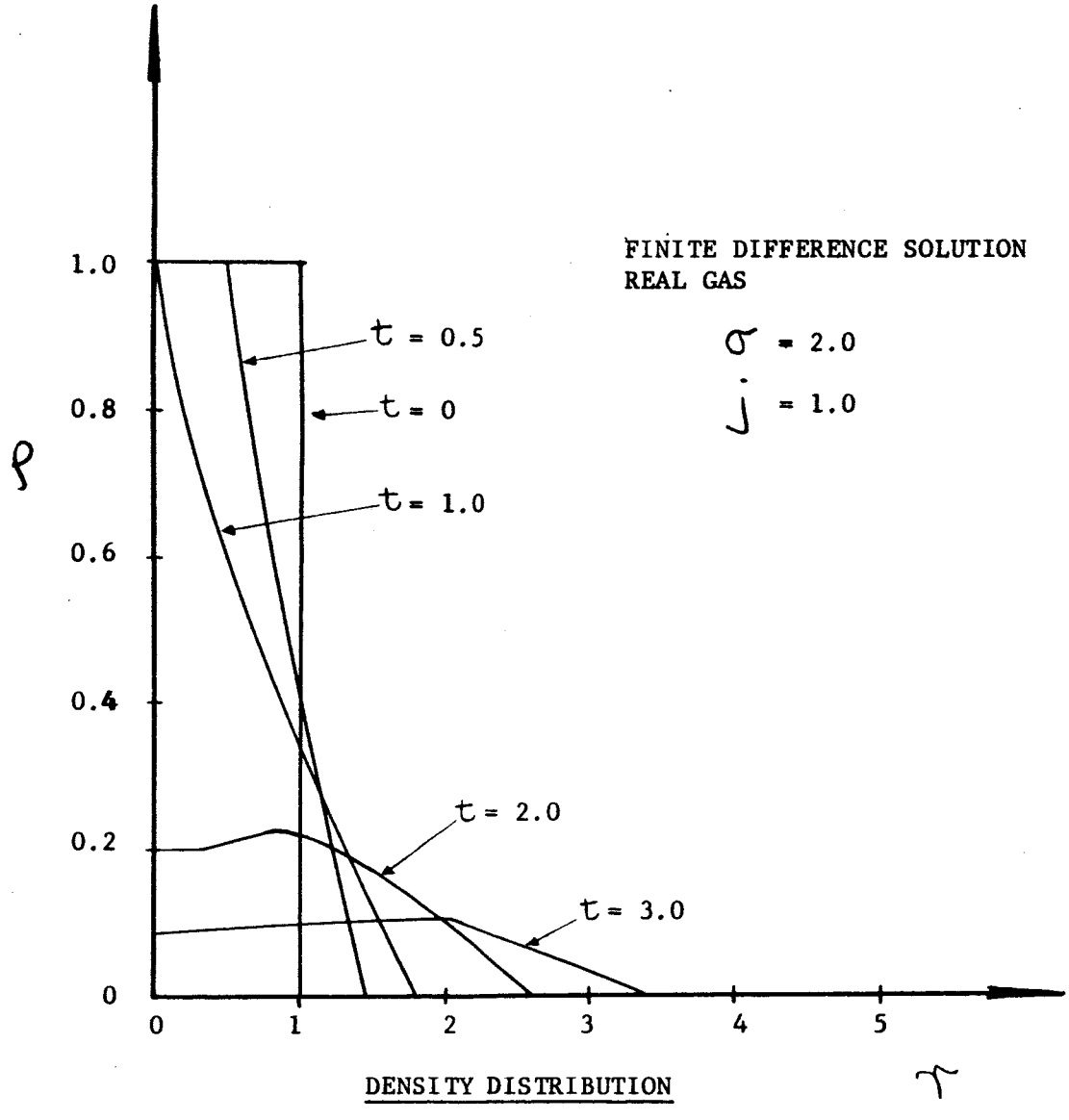

DENSITY DISTRIBUTION

FIG. 8.22

EFFECT OF TIME ON PARTICLE VELOCITY DISTRIBUTION

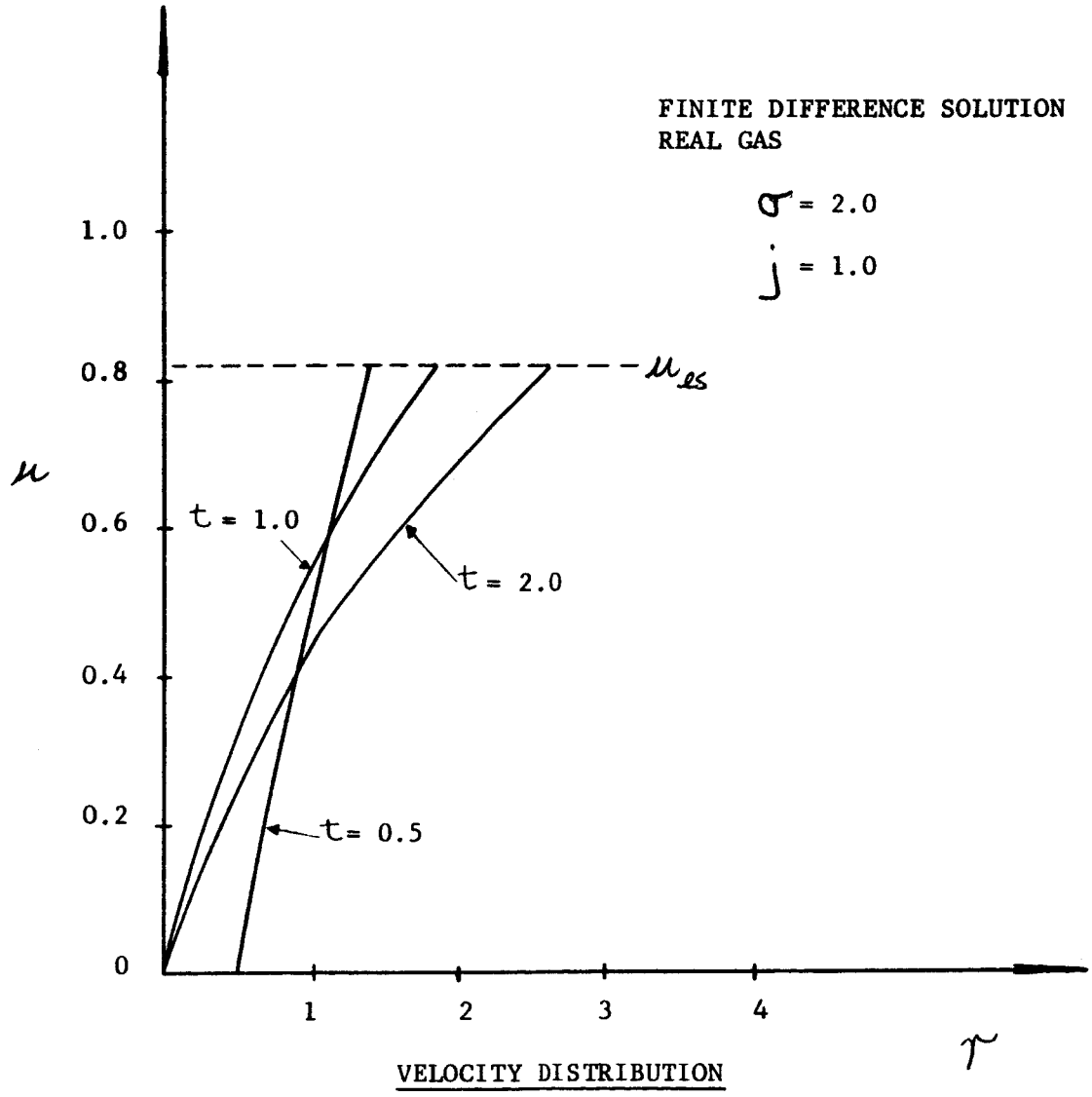

VELOCITY DISTRIBUTION

FIG. 8.23

COMPARISON OF REAL AND IDEAL GAS SOLUTIONS

FOR DENSITY DISTRIBUTION

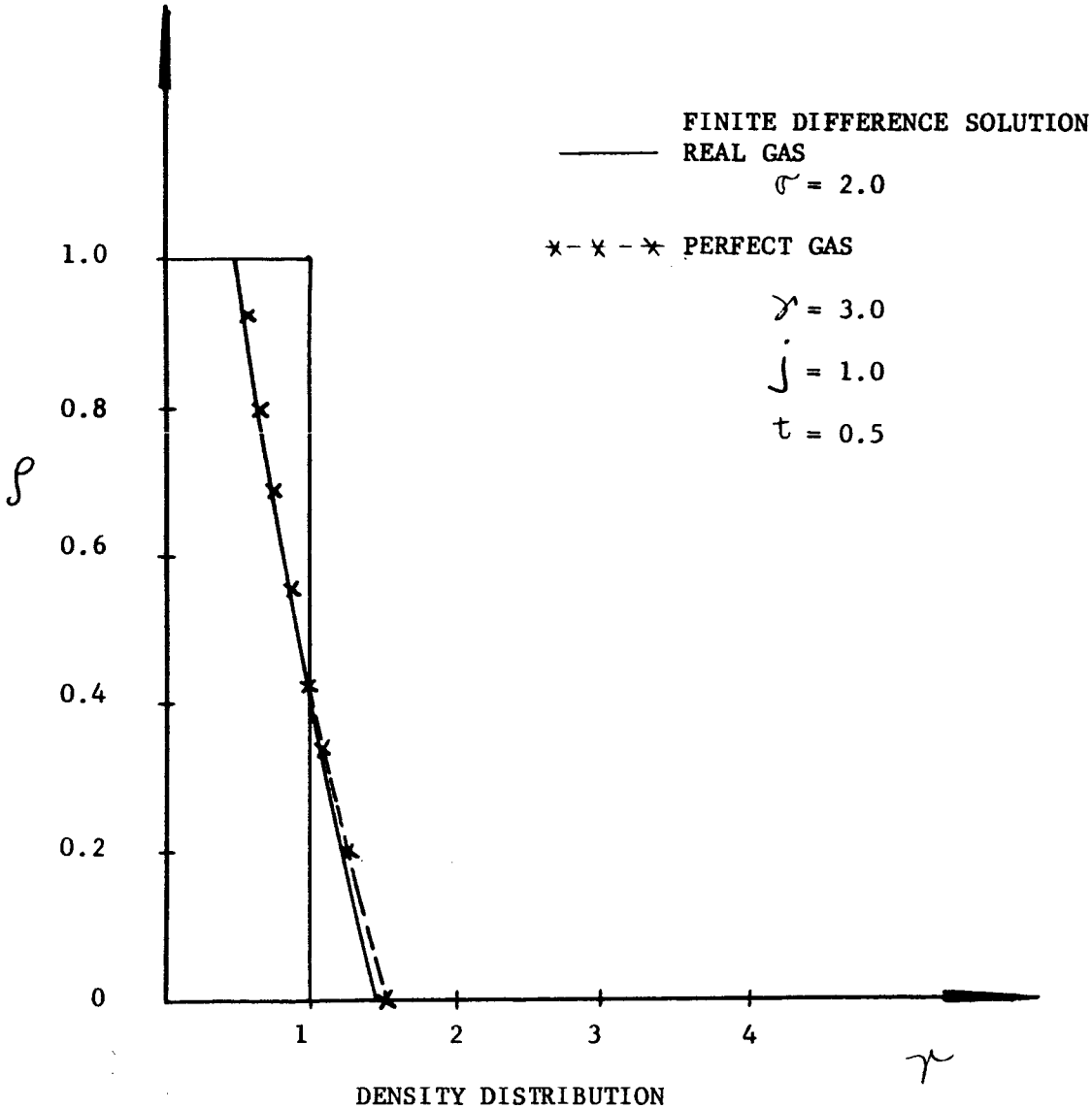

DENSITY DISTRIBUTION

FIG. 8.24

COMPARISON OF REAL AND IDEAL GAS SOLUTIONS FOR DENSITY DISTRIBUTION

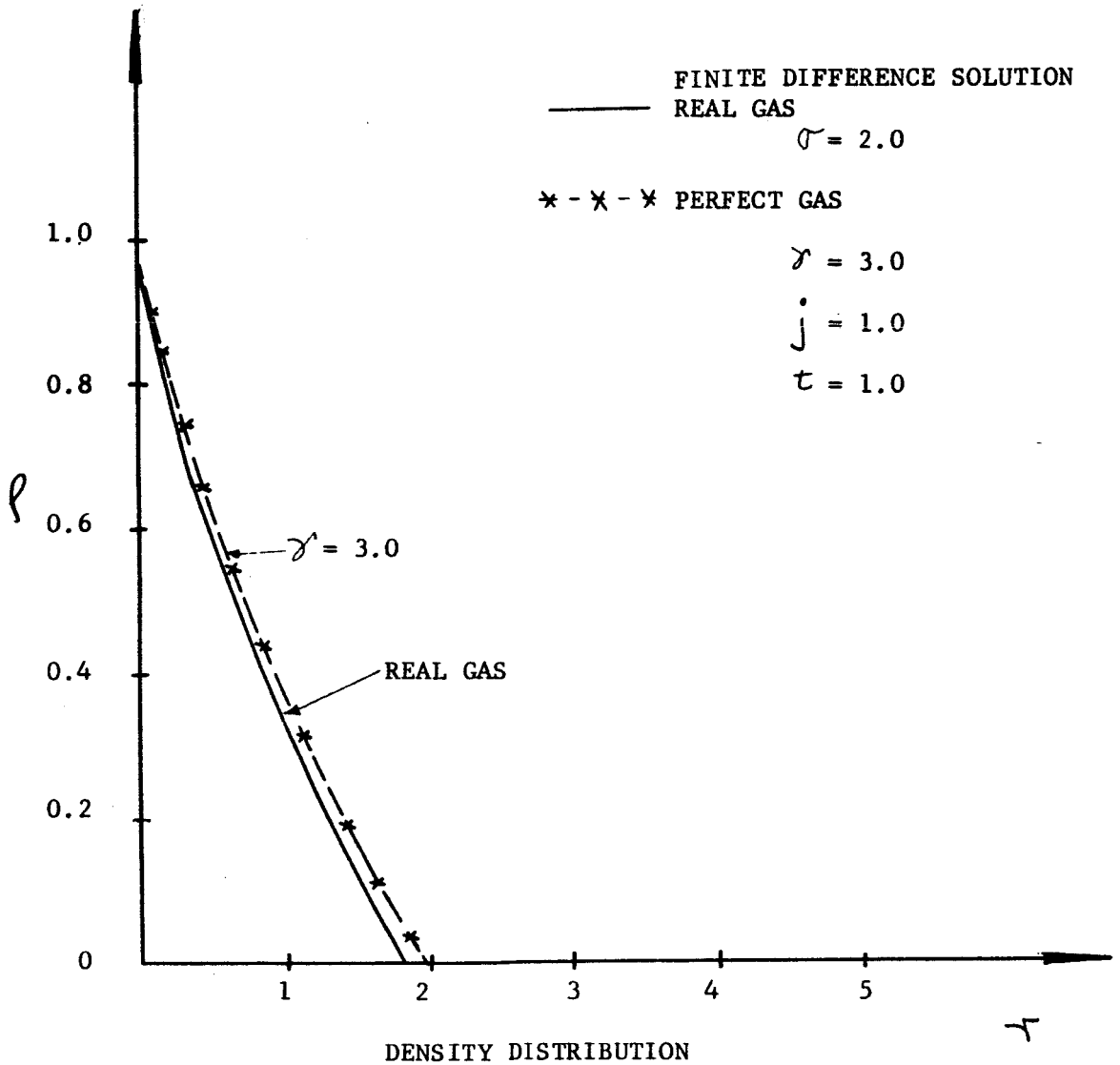

DENSITY DISTRIBUTION

FIG. 8.25

COMPARISON OF REAL AND IDEAL GAS SOLUTIONS

FOR DENSITY DISTRIBUTIONS

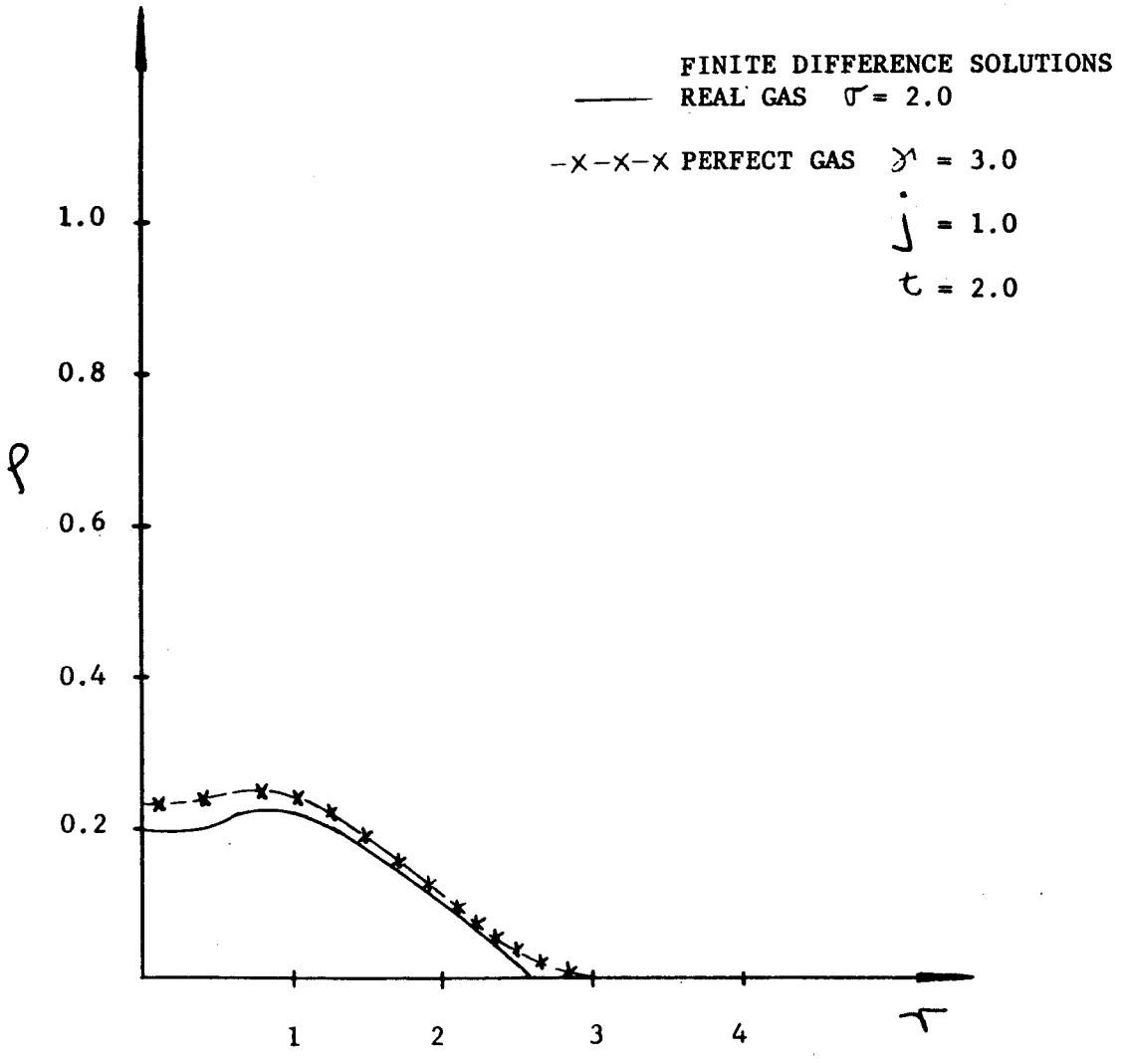

DENSITY DISTRIBUTION

FIG. 8.26

EFFECT OF TIME ON DENSITY DISTRIBUTION

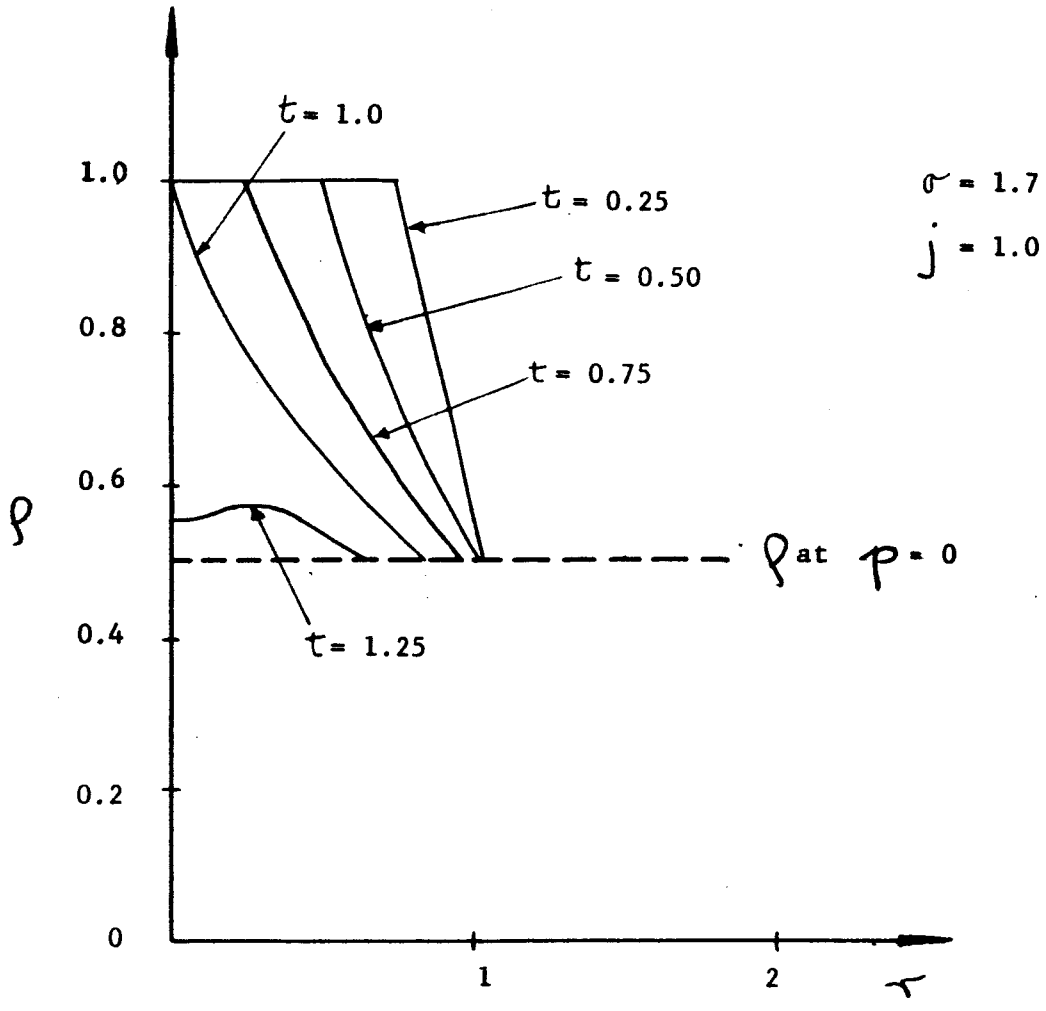

DENSITY DISTRIBUTION

FIG. 8.27

REFERENCES

1. Bull, G.V.: On the Impact of Pellets With Thin Plates McGill University, T.N. 1 - 10/61 (1961)

2. Walsh, J.M., Johnson, W.E., Dienes, J.K., Tillotson, J.H., Yates, D.R.: Summary Report on the Theory of Hypervelocity Impact. General Atomic GA-5119.

3. Keller, J.B.: Spherical, Cylindrical and One-Dimensional Gas Flows. Quart. App. Math. Vol. 14, No. 2,171 (1956).

4. Mirels, H. and Mullen, J.F.: Expansion of Gas Clouds and Hypersonic Jets Bounded By A Vacuum. AIAA Journal Vol. 1, No. 3,596 (1963).

TABLE 1

$\sigma = 2.0$

i	c_i	d_i	g_i
1	-0.0075342082	-0.089059629	0.51268487
2	0.0033611059	1.1313687	-0.50142606
3	1.8051498	0.00000	-0.023580486
4	-11.685586	0.00000	0.18603611
5	28.771736	0.00000	0.11303411
6	-26.840525	0.00000	-0.34116759
7	8.9565915	0.00000	-0.27784690

$$p = \sum_{i=1}^{7} c_i \rho^{i-1} \qquad \text{(isentrope)}$$

$$a = \sum_{i=1}^{7} d_i \rho^{i-1} \qquad \text{(isentrope)}$$

$$\rho = \sum_{i=1}^{7} g_i \left(\frac{\tau - 1}{\Delta}\right)^{i-1} \qquad \text{(starting conditions)}$$

TABLE 2

$\sigma = 1.7$

i	c_i	d_i	g_i
1	0.50557207	-275.41494	0.55002965
2	1.2407034	2109.7054	-0.21778543
3	-2.7742933	-6688.2209	0.44371078
4	5.8613678	11246.781	-0.041185003
5	-7.6545925	-10574.952	-0.60877374
6	5.3192251	5271.8190	-0.35783680
7	-1.4983452	-1088.7201	0.00000

$$p = \sum_{i=1}^{7} c_i \rho^{i-1} \qquad \text{(isentrope)}$$

$$a = \sum_{i=1}^{7} d_i \rho^{i-1} \qquad \text{(isentrope)}$$

$$\rho = \sum_{i=1}^{7} g_i \left(\frac{\tau - 1}{\Delta}\right)^{i-1} \qquad \text{(starting conditions)}$$